

Evaluation of Spin-Triplet Superconductivity in Sr_2RuO_4

Yoshiteru MAENO¹, Shunichiro KITTAKE^{1,2}, Takuji NOMURA³, Shingo YONEZAWA¹, and Kenji ISHIDA¹

¹*Department of Physics, Graduate School of Science, Kyoto University, Kyoto 606-8502, Japan*

²*Institute for Solid State Physics, University of Tokyo, Kashiwa, Chiba 277-8581, Japan*

³*Condensed Matter Science Division, Japan Atomic Energy Agency, Sayo, Hyogo 679-5148, Japan*

(Received December 30, 2011)

This review presents a summary and evaluations of the superconducting properties of the layered ruthenate Sr_2RuO_4 as they are known in the autumn of 2011. This paper appends the main progress that has been made since the preceding review by Mackenzie and Maeno was published in 2003. Here, special focus is placed on the critical evaluation of the spin-triplet, odd-parity pairing scenario applied to Sr_2RuO_4 . After an introduction to superconductors with possible odd-parity pairing, accumulated evidence for the pairing symmetry of Sr_2RuO_4 is examined. Then, significant recent progress on the theoretical approaches to the superconducting pairing by Coulomb repulsion is reviewed. A section is devoted to some experimental properties of Sr_2RuO_4 that seem to defy simple explanations in terms of currently available spin-triplet scenario. The next section deals with some new developments using eutectic boundaries and micro-crystals, which reveals novel superconducting phenomena related to chiral edge states, odd-frequency pairing states, and half-fluxoid states. Some of these properties are intimately connected with the properties as a topological superconductor. The article concludes with a summary of knowledge emerged from the study of Sr_2RuO_4 that are now more widely applied to understand the physics of other unconventional superconductors, as well as with a brief discussion of relatively unexplored but promising areas of ongoing and future studies of Sr_2RuO_4 .

KEYWORDS: Sr_2RuO_4 , ruthenate, spin-triplet superconductivity, topological superconductor

1. Spin-triplet superconductors

1.1 Candidates of Spin-triplet superconductors

In the last three decades, and particularly since the discovery of high-transition-temperature (high- T_c) superconductivity of the cuprates,¹ studies of “unconventional” superconductivity have been one of the main topics in condensed-matter physics. Here we designate the term “unconventional” as the pairing based on non-phonon mechanisms.² The unconventional superconductivity is mainly found in heavy-fermion superconductors (since 1978),³ high- T_c cuprates (since 1986),¹ organic superconductors (since 1980),⁴ ruthenate superconductors (since 1994),⁵ and iron-pnictide superconductors (since 2008).⁶ Unconventional superconductivity is characterized by the anisotropic gap function or order parameter which is integrated to be zero or a small value due to the variations of the wave function “phase”, in contrast to an ordinary s -wave state. In many of them, including high- T_c cuprates and iron pnictides, the electrons are clearly paired in *spin-singlet* states. In this point of view, they are similar to conventional s -wave superconductors, in which the spin-degrees of freedom is lost in the charged superfluids. *Spin-triplet* superfluid states are fully established in the Fermi liquid ^3He ,^{7,8} for which spin and mass supercurrents emerge in the charge-neutral superfluids. The question is then whether or not spin-triplet *superconductors* exist, and what novel superconducting properties they may exhibit due to their charge and spin supercurrents.

There are several classes of candidates of spin-triplet superconductors represented in Table III. We should note

here that due to strong spin-orbit interactions of heavy elements, spin is not a good quantum number in the f -electron based heavy fermions; their possible pseudo-spin-triplet pairing may be better termed as “odd-parity” pairing for their orbital wave function symmetry. Keeping this in mind, we will nevertheless use the term “spin-triplet” whenever it causes no confusion. Among the heavy fermions, UPt_3 is the leading candidate of a triplet superconductor.⁹ The measurements of spin susceptibility indicate that pairing in UNi_2Al_3 ¹⁰ is also triplet,¹¹ whereas the pairing in UPd_2Al_3 is clearly spin-singlet.^{12,13} Recent progress in the studies of ferromagnetic heavy-fermion superconductors such as UGe_2 ,¹⁴ URhGe ,¹⁵ and UIr ,¹⁶ and in particular UCoGe ,¹⁷ motivates researchers to seek for obtaining direct evidence for spin-triplet pairing.

Among the organic superconductors, possible spin-triplet pairing in quasi-one-dimensional superconductors $(\text{TMTSF})_2\text{X}$ ($\text{X} = \text{ClO}_4$ and PF_6) has been considered.^{30,31} However, spin-singlet pairing is demonstrated by nuclear magnetic resonance (NMR) Knight shift for $\text{X} = \text{ClO}_4$.³² In addition, recent results of detailed field-orientation dependence of the onset temperature derived from resistivity indicate that the unusual survival of superconductivity in high magnetic fields is attributable to the formation of the Fulde-Ferrell-Larkin-Ovchinnikov (FFLO) state of spin-singlet superconductivity.^{33,34}

A new class of spin-triplet pairing has been recognized in some superconductors having crystal structures without inversion symmetry, such as $\text{Li}_2\text{Pt}_3\text{B}$.²⁴ It is believed that if the spin-orbit splitting of the Fermi surfaces due to internal elec-

Table I. Selection of candidates of spin-triplet superconductors. HF: heavy fermion superconductors, NCS: Noncentrosymmetric superconductors, FM: ferromagnetic superconductors, *: superconductivity under pressure.

Materials	Classification	Spin evidence of triplet pairing	Properties
^3He	Superfluid	magnetization, NMR etc. ⁷	p -wave, A phase is chiral
Sr_2RuO_4	Oxide	NMR, polarized neutron	2D analogue of $^3\text{He-A}$
UPt_3	HF	NMR ¹⁸	Chiral p -wave
UBe_{13} , URu_2Si_2 , UNi_2Al_3	HF	NMR ¹³	f -wave
UGe_2^* , URhGe , UCoGe	FM, HF	Indirect	Anomalous H_{c2} ¹⁹⁻²²
UIr^*	NCS, FM, HF	Indirect	
CeIrSi_3^*	NCS, HF	NMR ²³	
$\text{Li}_2\text{Pt}_3\text{B}$	NCS	NMR ²⁴	
CePt_3Si	NCS, HF	Indirect	
CeRhSi_3^*	NCS, HF	Indirect	Anomalous H_{c2} ²⁵
S/FM/S	junctions	Indirect (I_c) ²⁶⁻²⁹	Odd-freq., even-parity, s -wave

tric fields exceeds the superconducting gap energy, the pairing state is no longer classified as purely spin-singlet or triplet, but their mixing occurs.^{35,36} As a result, a variety of unusual behavior characteristic of spin-triplet pairing such as extremely high upper critical field H_{c2} emerges. Examples are CePt_3Si ,³⁷ CeRhSi_3 ,³⁸ etc. In particular, anisotropic spin susceptibility in the superconducting state has been reported for CeIrSi_3 .²³ As Mukuda *et al.* explained, if the spin susceptibility is dominated by strong Rashba-type spin-orbit coupling, Knight-shift measurements do not give direct evidence for the admixture between the Cooper-pairing states of even and odd parity. The anisotropy may well be dominated by that of Van-Vleck-like susceptibility.

Sr_2RuO_4 , the main subject of this review, is the first oxide superconductor in the same layered structure as high- T_c cuprates but with a low superconducting transition temperature of 1.5 K.^{5,39} The availability of high-quality single crystals and the relative simplicity of its fully-characterized Fermi surfaces promoted a large number of experimental as well as theoretical studies. Sr_2RuO_4 is now established as one of the archetypal unconventional superconductors. In particular, it is considered most probably as a spin-triplet superconductor, comparable with the odd-parity, pseudo-spin-triplet superconductor UPt_3 .⁴⁰

We should add that the emergence of spin-triplet pairing states is also discussed in superconductor-ferromagnet-superconductor (S/FM/S) junctions. By the proximity effect into ferromagnetic half-metal such as CrO_2 , s -wave pair amplitude may penetrate as spin-triplet s -wave state.^{26,27} Such an unusual state is known as odd-frequency pairing.⁴¹ Recently, the long-range proximity effect due to odd-frequency spin-triplet currents is also demonstrated using ferromagnetic hybrid layers with some disorder and rotation of magnetization.^{28,29}

1.2 Unconventional superconducting properties of Sr_2RuO_4

From its Fermi surface topography and H_{c2} anisotropy, Sr_2RuO_4 is characterized as a highly anisotropic superconductor with the anisotropy ratio of 20. Nevertheless, the out-of-plane coherence length ξ_c is several times greater than the interlayer distance to allow interlayer coherence. Table II summarizes basic superconducting parameters obtained mainly from the anisotropic H_{c2} and the specific heat. We note that the evaluation of ξ_c assumes orbital limiting of H_{c2} .

Sr_2RuO_4 exhibits a number of phenomena reflecting its unconventional superconductivity. The extreme sensitivity to non-magnetic impurities and defects indicates non- s -wave pairing with sign-changes on the superconducting gap. In fact the transition temperature T_c diminishes at the impurity concentration at which the mean impurity-impurity distance becomes comparable to the in-plane coherence length ξ_{ab} , consistent with the modified Abrikosov-Gorkov prediction.^{42,43} Absence of coherence peak (Hebel-Schlichter peak) and the power-law temperature dependence in the NMR spin-lattice relaxation rate $1/T_1$ indicate non- s -wave with highly anisotropic gap structure.⁴⁴ The magnetic field dependence of the specific heat at low temperatures reveals a plateau in the intermediate H , indicative of the multi-gap superconductivity reflecting the existence of three Fermi surfaces with different orbital characters.⁴⁵

It should be mentioned that the theoretical proposal for the similarity between the superconductivity of Sr_2RuO_4 and the spin-triplet superfluidity of ^3He soon after the discovery of ruthenate superconductivity⁴⁶ strongly motivated the experimental efforts to determine the symmetry of unconventional superconductivity in Sr_2RuO_4 . This leads to the first direct experimental evidence of spin-triplet pairing in Sr_2RuO_4 by the measurements of the electron spin susceptibility with NMR.⁴⁷ Combined with the observation of internal magnetic field by μSR ,⁴⁸ this result yields a complete description of the superconducting state of Sr_2RuO_4 as a two-dimensional analogue

Table III. Selection of candidates of spin-triplet superconductors. HF: heavy fermion superconductors, NCS: Noncentrosymmetric superconductors, FM: ferromagnetic superconductors, *: superconductivity under pressure.

Materials	Classification	Spin evidence of triplet pairing	Properties
${}^3\text{He}$	Superfluid	magnetization, NMR etc. ⁷	p -wave, A phase is chiral
Sr_2RuO_4	Oxide	NMR, polarized neutron	2D analogue of ${}^3\text{He}$ -A
UPt_3	HF	NMR ¹⁸	Chiral p -wave
UBe_{13} , URu_2Si_2 , UNi_2Al_3	HF	NMR ¹³	f -wave
UGe_2^* , URhGe , UCoGe	FM, HF	Indirect	Anomalous H_{c2} ¹⁹⁻²²
UIr^*	NCS, FM, HF	Indirect	
CeIrSi_3^*	NCS, HF	NMR ²³	
$\text{Li}_2\text{Pt}_3\text{B}$	NCS	NMR ²⁴	
CePt_3Si	NCS, HF	Indirect	
CeRhSi_3^*	NCS, HF	Indirect	Anomalous H_{c2} ²⁵
S/FM/S	junctions	Indirect (I_c) ²⁶⁻²⁹	Odd-freq., even-parity, s -wave

Table II. Superconducting parameters for Sr_2RuO_4 . H_c is the thermodynamical critical field, ξ is the coherence length, λ is the penetration depth, and κ is the Ginzburg-Landau parameter. *Conventional orbital depairing for H_{c2} is assumed.

Parameter		ab	c
T_c	(K)	1.50	
$\mu_0 H_{c2}(0)$	(T)	1.50	0.075
$\mu_0 H_c(0)$	(T)	0.023	
$\xi(0)$	(Å)	660	33*
$\lambda(0)$	(Å)	1900	3.0×10^4
$\kappa(0)$		2.6	46
ξ_{ab}/ξ_c		20	

of the ${}^3\text{He}$ -A phase, i.e., a spin-triplet chiral p -wave state.⁴⁹

1.3 Scope of this review

There have been several review articles devoted to the superconductivity of Sr_2RuO_4 .^{39,44,50,51} In addition, we mention a review on the Fermi-liquid properties in the normal state⁵² and stories behind the discovery of its superconductivity.^{53,54} Especially, an extensive review of the developments up to the spring of 2002 by Mackenzie and Maeno has been cited more than 500 times. Since then, much research progress has been made on Sr_2RuO_4 in both experiments and theories, especially concerning the superconducting gap structure, the order-parameter symmetry, and the properties of superconducting states in junctions and at boundaries.

The purpose of this review is to make a critical examination of the spin-triplet pairing scenario of Sr_2RuO_4 , in order to fully understand the behavior of such superconducting state. The ideas emerged from the studies of Sr_2RuO_4 include multi-gap superconductivity of multi-band systems, physics of superconductivity with time-reversal symmetry breaking, pairing mechanism in highly correlated materials in which

spin fluctuation is not necessarily strong. Such analysis should help understanding the properties of other unconventional superconductors, and moreover help resolving some of the long standing remaining issues of spin-triplet superfluid ${}^3\text{He}$.⁴⁰

In § 2, we first introduce the order parameter of spin-triplet superconductivity, the d -vector, especially the d -vector states relevant to the superconductivity of Sr_2RuO_4 . We examine the experimental evidence for spin-triplet pairing based on traditional probes, but with innovative approaches. A variety of NMR Knight-shift experiments and polarized neutron experiments establish the spin-triplet pairing. We also address alternative possibilities of the d -vector orientation consistent with the NMR. We then describe experiments establishing the time-reversal symmetry breaking, or chiral nature, of the order parameter.

Section 3 summarizes the theoretical advancement in unconventional pairing mechanism by Coulomb repulsion. The importance of non-boson exchange, namely vertex-correction processes, is emphasized. We also review and examine other approaches to the unconventional pairing mechanism for Sr_2RuO_4 . The important roles played by the spin-orbit interaction, which determines the direction of the d -vector, are also discussed.

Section 4 deals with the superconducting properties of Sr_2RuO_4 which remain unresolved within the current theoretical models. These are the origin of the strong suppression of H_{c2} with the fields parallel to the RuO_2 plane and the emergence of a second superconducting phase at low temperatures under the same condition.

Section 5 describes novel superconducting phenomena in Sr_2RuO_4 , such as enhanced superconductivity (the so-called 3-K phase) at the interface between Sr_2RuO_4 and Ru in the eutectic system, and novel proximity effects in various superconducting junctions involving Sr_2RuO_4 . Descriptions of Andreev bound states in terms of odd-frequency pairing and chiral edge states are introduced. Many of these phenomena

are characteristics of a topological superconductor. We also describe the current experimental status of observing half-fluxoid states in micron-scale rings of Sr_2RuO_4 crystals and discuss the physics of half-quantum vortices in spin-triplet superconductors.

Finally in § 6, we summarize the present status towards establishing the spin-triplet superconductivity in Sr_2RuO_4 and discuss the future prospects of the physics of topological superconductivity.

2. Evidence for spin triplet pairing

2.1 Order parameter of spin-triplet superconductivity: the d -vector

We start with a useful description of the order parameter of spin-triplet superconductivity, namely the d -vector. The superconducting order parameter is given by a function of spin and momentum in general: $\Delta_{\sigma\sigma'}(\mathbf{k})$. Roughly speaking, $\Delta_{\sigma\sigma'}(\mathbf{k})$ is regarded as a wave function of a Cooper pair formed by two quasi-particles whose momenta and spins are (\mathbf{k}, σ) and $(-\mathbf{k}, \sigma')$. The magnitude of the total spin of a Cooper pair is $S = 1$ in spin-triplet pairing, in contrast to $S = 0$ in spin-singlet pairing. In spin-triplet pairing, the degrees of freedom about the direction of the spin $S = 1$ remain even in the superconducting state. For spin-triplet pairing, $\Delta_{\sigma\sigma'}(\mathbf{k})$ is expressed using the d -vector as:⁵⁵

$$\Delta_{\sigma\sigma'}(\mathbf{k}) = i[(\mathbf{d}(\mathbf{k}) \cdot \boldsymbol{\sigma})\sigma_y]_{\sigma\sigma'}, \quad (1)$$

or

$$\begin{pmatrix} \Delta_{\uparrow\uparrow}(\mathbf{k}) & \Delta_{\uparrow\downarrow}(\mathbf{k}) \\ \Delta_{\downarrow\uparrow}(\mathbf{k}) & \Delta_{\downarrow\downarrow}(\mathbf{k}) \end{pmatrix} = \begin{pmatrix} -d_x(\mathbf{k}) + id_y(\mathbf{k}) & d_z(\mathbf{k}) \\ d_z(\mathbf{k}) & d_x(\mathbf{k}) + id_y(\mathbf{k}) \end{pmatrix}, \quad (2)$$

where $\boldsymbol{\sigma}$ is the Pauli spin matrix vector: $\boldsymbol{\sigma} = (\sigma_x, \sigma_y, \sigma_z)$. The order parameter of triplet pairing states is described completely by the three components of the d -vector $\mathbf{d}(\mathbf{k})$. $\mathbf{d}(\mathbf{k})$ is an odd-parity function of \mathbf{k} . The d -vector behaves as a vector under rotations in spin space. Here we should note that the direction of the d -vector is perpendicular to the total spin S of a Cooper pair. To see this simply, we consider the case of $\mathbf{d} \parallel z$, i.e., $\mathbf{d}(\mathbf{k}) = (0, 0, d_z(\mathbf{k}))$. Then we have $\Delta_{\uparrow\uparrow}(\mathbf{k}) = \Delta_{\downarrow\downarrow}(\mathbf{k}) = 0$, i.e., $S_z = 0$, which means $\mathbf{d} \perp \mathbf{S}$. In general, each component of the d -vector (d_x , d_y , or d_z) represents the pair amplitude with the Cooper-pair spin perpendicular to the corresponding basis (\hat{x} , \hat{y} , or \hat{z}). Triplet pairing states satisfying $\mathbf{d}(\mathbf{k}) \times \mathbf{d}^*(\mathbf{k}) = 0$ ($\mathbf{d}(\mathbf{k}) \times \mathbf{d}^*(\mathbf{k}) \neq 0$) are called *unitary* (*non-unitary*) states. In non-unitary states, spins of the Cooper pairs are polarized. We can see this simply by considering the quantity $|\Delta_{\uparrow\uparrow}(\mathbf{k})|^2 - |\Delta_{\downarrow\downarrow}(\mathbf{k})|^2 = 2i[\mathbf{d}(\mathbf{k}) \times \mathbf{d}^*(\mathbf{k})]_z \neq 0$ for non-unitary states.

The order parameters of superfluid phases of ^3He are expressed as:⁵⁶ $\mathbf{d}(\mathbf{k}) \propto \hat{z}(k_x \pm ik_y)$ (A phase), $\mathbf{d}(\mathbf{k}) \propto \hat{x}k_x + \hat{y}k_y + \hat{z}k_z$ (B phase), $\mathbf{d}(\mathbf{k}) \propto (\hat{x} + i\hat{y})(k_x + ik_y)$ (A1 phase emerging under magnetic fields). Both of the A and B phases are unitary states, while the A1 phase is a non-unitary state with spin po-

larization. For the state $\mathbf{d}(\mathbf{k}) \propto \hat{z}(k_x \pm ik_y)$, we can choose a new spin coordinate system in which $\Delta_{\uparrow\downarrow}(\mathbf{k}) = \Delta_{\downarrow\uparrow}(\mathbf{k}) = 0$, i.e., $d_z(\mathbf{k}) = 0$ at all \mathbf{k} . To see this, we rotate the spin coordinate system by $2\pi/3$ around the $[111]$ axis. Then the basis vectors \hat{x} , \hat{y} and \hat{z} are transferred to \hat{z} , \hat{x} and \hat{y} , respectively, and consequently we have $d_z(\mathbf{k}) = d_x(\mathbf{k}) = 0$ for all \mathbf{k} in the new spin coordinate system. In general, if we can choose appropriate spin coordinates by which $d_z(\mathbf{k}) = 0$ for all \mathbf{k} , then we call the pairing state ‘‘equal-spin pairing’’ (ESP) state. The A and A1 phases are ESP states, while the B phase is not. For those not familiar with the description of the spin-triplet order parameter, the review by Mackenzie and Maeno (§ IV and Appendix D), as well as the Appendix of this review, gives an introductory but more detailed treatment in terms of the d -vector. For example, one can find the relation between the spin bases and the d -vector bases, and the expression of the superconducting gap in terms of the d -vector.

Down to the low temperatures, Sr_2RuO_4 maintains a tetragonal structure with the crystal point group symmetry D_{4h} .⁵⁷ Neglecting the dispersion along the out-of-plane c direction, possible spin-triplet states are limited to those for the two-dimensional square lattice with C_{4v} symmetry and are given in Table IV. Figures 1(a) and 1(b) depict the Γ_1 and Γ_5 states, respectively. The former can be thought of as the quantum-mechanical superposition of the two states with antiparallel combinations of spin and orbital wave functions, with quenched overall orbital angular momentum:

$$\mathbf{d}(\mathbf{k}) \propto (\hat{x} + i\hat{y})(k_x - ik_y) + (\hat{x} - i\hat{y})(k_x + ik_y) \quad (3)$$

The d -vector $\hat{x} \pm i\hat{y}$ lies in the basal plane, which for illustrative purpose is depicted by yellow arrows in Fig. 1(a). The Γ_5^- states in Table IV are called the *chiral pairing* states, because these states possess two polarizations of relative orbital angular momentum of pairing quasi-particles: left- and right-handed polarizations correspond to $k_x + ik_y$ and $k_x - ik_y$, respectively. They are the states with the orbital angular momentum $L_z = +1$ or -1 as represented by big arrows in Fig. 1(b); the Cooper-pair spins lie in the basal plane as $\mathbf{d} \perp \mathbf{S}$. We note that all five states $\Gamma_1 - \Gamma_5$ are the so-called ESP states, for which the spin state of the Cooper pair is always a linear superposition of $S_z = +1$ and $S_z = -1$ states by a suitable choice of spin axes.

2.2 Spin part of the order parameter

The direct evidence for spin-triplet pairing in Sr_2RuO_4 is based mainly on the following two kinds of experiments. One is the electronic spin susceptibility measurements by the NMR Knight shifts of both ^{17}O and ^{99}Ru nuclei.^{47,58} The other evidence comes from the measurements of local magnetization by polarized neutron diffraction; the so-called Shull-Wedgewood experiments.⁵⁹

In this subsection, we focus on the NMR experiments in some detail. The NMR Knight shift measures the effective field at the nucleus produced by the electrons, and thus is related to the microscopic spin susceptibility at the NMR nuclear site. Since the spin susceptibility in the superconducting

Table IV. List of possible five d -vector states⁴⁶ for Sr_2RuO_4 . Irreducible representations of the C_{4v} symmetry group are displayed by both of the Bethe and Mulliken notations in the first two columns. The minus sign in the Bethe notation and the index “ u ” (denoting *ungerade*) in the Mulliken notation represent odd parity. TRSB in the fifth column means time-reversal symmetry breaking. Γ_1^- and Γ_5^- are analogous states to the $^3\text{He-B}$ and $^3\text{He-A}$ phases, respectively. Γ_5^- corresponds to the chiral p -wave state. In the absence of the spin-orbit interaction among Ru- $4d$ electrons, i.e., assuming isotropy in spin space, any superpositions of these five states are also possible. Note that the column “ d -vector” displays only the symmetry of $\mathbf{d}(\mathbf{k})$ as a function of \mathbf{k} . For example, if we take the functions $\sin k_x$ and $\sin k_y$ for the k_x - and k_y -symmetry, then we have $\mathbf{d}(\mathbf{k}) \propto \hat{z}(\sin k_x \pm i \sin k_y)$ for Γ_5^- . All of the five states are unitary ESP states, and give full energy gap at the Fermi level.

Bethe	Mulliken	d -vector	direction of \mathbf{d}	TRSB	Analogy to ^3He
Γ_1^-	A_{1u}	$\hat{x}k_x + \hat{y}k_y$	$\mathbf{d} \parallel ab$	No	BW state (B phase)
Γ_2^-	A_{2u}	$\hat{x}k_y - \hat{y}k_x$	$\mathbf{d} \parallel ab$	No	
Γ_3^-	B_{1u}	$\hat{x}k_x - \hat{y}k_y$	$\mathbf{d} \parallel ab$	No	
Γ_4^-	B_{2u}	$\hat{x}k_y + \hat{y}k_x$	$\mathbf{d} \parallel ab$	No	
Γ_5^-	E_u	$\hat{z}(k_x \pm ik_y)$	$\mathbf{d} \parallel c$	Yes	ABM state (A phase)

state cannot be extracted from the bulk susceptibility due to the Meissner shielding, the Knight-shift measurement is considered as the most reliable method to measure the spin susceptibility in the superconducting state.⁴⁴

The Cooper pair spin susceptibility of Sr_2RuO_4 can be reliably extracted from the NMR Knight shift K for the following reasons. First, the NMR and nuclear quadrupole resonance (NQR) measurements have been performed on a variety of nuclei, three different crystal sites of ^{17}O (NMR and NQR), ^{99}Ru (NMR), and ^{101}Ru (NQR), covering wide parameter range in the field-temperature (H - T) phase diagram. Thus accidental signal cancellation due to the structure factor is avoided. In addition, it is noticeable that one can also obtain the bulk susceptibility and nuclear spin-lattice relaxation rate ($1/T_1$) within the same measurement setup. This fact enables us to carefully check the consistency of the data from different viewpoints. Second, overheating of the sample by RF pulses is avoided by monitoring the intensity of the NMR peak itself, thereby using the NMR nuclei as an internal thermometer (Supplement of Ref. 47). Third, based on the systematic studies of K among different ruthenates, i.e., RuO_2 , Sr_2RuO_4 , and CaRuO_3 , it is clear that a large negative value of K for Sr_2RuO_4 originates from the contribution from core polarization due to d -electrons (Fig. 2).⁶⁰ From such analysis, the contribution from the orbital part is estimated as 1.0% while the spin contribution is -4.5% for $K \parallel c$ of Sr_2RuO_4 . With the anisotropy of the spin part of only 2% as extracted from the χ_{ab} vs χ_c plot,⁶¹ the dominance of the spin part in the susceptibility^{62,63} is illustrated in Fig. 3. Such properties of Sr_2RuO_4 ensure that its NMR Knight shift serves as a reliable high-sensitivity probe for the Cooper pair spin susceptibility.

Ishida and coworkers have measured Knight shifts $K(T)$ at the Ru and O sites in high-quality single crystals. Measurements were performed using a ^3He - ^4He dilution refrigerator with the sample crystals directly immersed in liquid helium to ensure good thermal contact to the bath. As for the ^{17}O Knight-shift measurements, they assigned NMR signals arising from the different crystal sites (planer and apical O sites), and estimated the spin part of the Knight shift above T_c at each site. They investigated temperature depen-

dence of the Knight shift at the planer O site, where the spin density is 6 times larger than that in the apical O site, and showed that its Knight shift remains unchanged in the field range ($0.35 \text{ T} < \mu_0 H < 1.1 \text{ T}$) applied parallel to the RuO_2 plane.⁴⁷

They also measured the Knight shift at the Ru site in the RuO_2 plane. The advantage of the Ru Knight shift measurements is that the value of the ^{99}Ru Knight shift is an order of magnitude larger than that of the ^{17}O Knight shift, since the ^{99}Ru shift is strongly affected by Ru- $4d$ electronic spins through the large hyperfine coupling constant of $A_{\text{cp}} = -25 \text{ T}/\mu_B$ originating from the core polarization effect, where μ_B is the Bohr magneton. This means that the Ru Knight shift can detect much smaller changes of the Ru- $4d$ electronic state when superconductivity sets in. The temperature dependence of the ^{99}Ru shift was measured in the fields of 0.68, 0.9, and 1.05 T parallel to the RuO_2 plane and the spin part of the Knight shift ($^{99}K_{\text{spin}} = K(T) - K_{\text{orb}}$) obtained at 0.9 T is shown in Fig. 4.

$^{99}K_{\text{spin}}$ does not change on passing through $T_c \sim 1.0 \text{ K}$ at $\mu_0 H \sim 0.9 \text{ T}$. If a spin-singlet d -wave state with a line-node gap were realized, the T dependence of $^{99}K_{\text{spin}}$ would behave as drawn by the dashed curve in Fig. 4. Here we adopted the magnitude of the gap $2\Delta_0 = 4k_B T_c$, which has been used for analyses of various physical quantities. It is obvious that the unchanged Knight shift in the superconducting state at both the O and Ru sites in the RuO_2 plane cannot be understood by the spin-singlet scenarios, but strongly suggests the Cooper-pair spins are in the triplet state and can be polarized to the applied field parallel to the RuO_2 plane.

In general, the spin susceptibility in the spin-triplet superconducting state is expected to show anisotropic temperature dependence reflecting the magnitude and direction of the applied field. When the interaction acting on the triplet pairs is strong enough to lock the spins of a superconducting pair in a certain direction of the crystal, the anisotropy of the spin susceptibility, i.e., the anisotropic behavior of the Knight shift should be observed in the superconducting state. The Knight shift is unchanged when magnetic fields are parallel to the spin direction ($\mathbf{d} \perp H$). But when magnetic fields

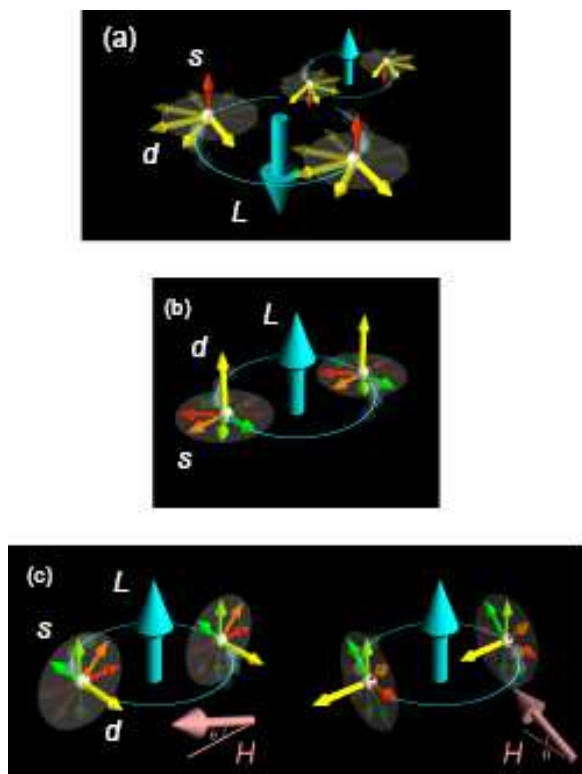


Fig. 1. (Color online) Illustrations of Cooper-pair spins and orbital angular momenta for spin-triplet superconductivity. The Cooper-pair spins S are depicted by small arrows in various colors; the d -vector shown by yellow arrows is defined perpendicular to the spins. The orbital angular momentum L of a Cooper pair is shown by a large blue arrow. (a) The S and L vectors for the Γ_1 state, $\mathbf{d}(\mathbf{k}) = \Delta_0(\hat{x}k_x + \hat{y}k_y)$. It can be thought of as a quantum-mechanical superposition of $S_z = +1$ and $S_z = -1$ states (see text). (b) The promising ground state $\mathbf{d}(\mathbf{k}) = \hat{z}\Delta_0(k_x + ik_y)$ with the d -vector pointing in the c direction. (c) Possible states under magnetic fields. The d -vector rotates within the basal plane in response to the external magnetic fields. The Cooper-pair spins can be polarized by magnetic fields of any directions.

are applied perpendicular to the spin direction ($\mathbf{d} \parallel \mathbf{H}$), the Knight shift decreases depending on the superconducting gap structure. On the other hand, if the energy of the pinning interaction is weaker so that the spins can reorient easily toward the applied magnetic field, the Knight shift is invariant in any field direction. Thus the Knight shift measurements in small fields are important to understand the pinning interaction of the d -vector.

In order to measure the Knight shift in such small fields, Murakawa *et al.* employed a ^{101}Ru NQR spectrum for observing the signals, and measured the Knight shift at the Ru site^{63,64} as shown in Fig. 5(a). They measured the temperature dependence of the resonance frequency of the Ru NQR signal affected by the applied field parallel to the RuO_2 plane. The expected decrease of the spin susceptibility in the case of the spin-singlet pairing or spin-triplet with the d -vector in the RuO_2 plane is shown by the dotted curve. Obviously such suppression was not observed, and the spin susceptibility is in-

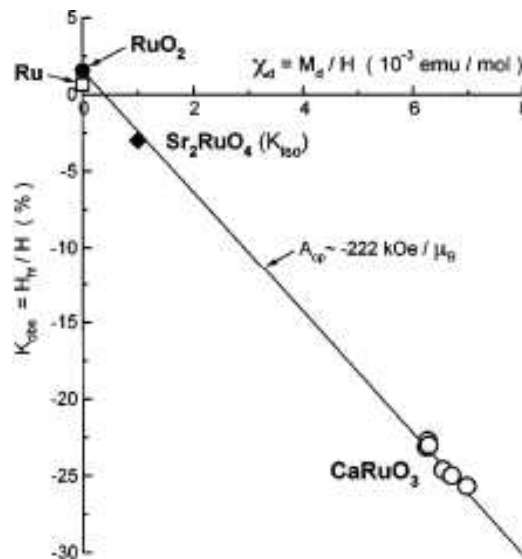


Fig. 2. Knight shift vs bulk susceptibility determined in the range $T = 1.4 - 20$ K for a weakly-correlated metal RuO_2 , an electron-correlated superconductor Sr_2RuO_4 , and a correlated, nearly ferromagnetic metal CaRuO_3 . The hyperfine coupling constant due to the inner core polarization $A_{\text{cp}} \sim -22.2 \text{ T}/\mu_B$ is estimated from a linear slope with the assumption that $K_{\text{orb}} = 1.59\%$ is common among these ruthenates. The value of A_{cp} is close to $A_{\text{hf}} \sim 30 \text{ T}/\mu_B$ in the FM state of SrRuO_3 . A large negative K value of Sr_2RuO_4 indicates that its susceptibility is dominated by the d -electron spin susceptibility (Fig. 5 in Ref. 60).

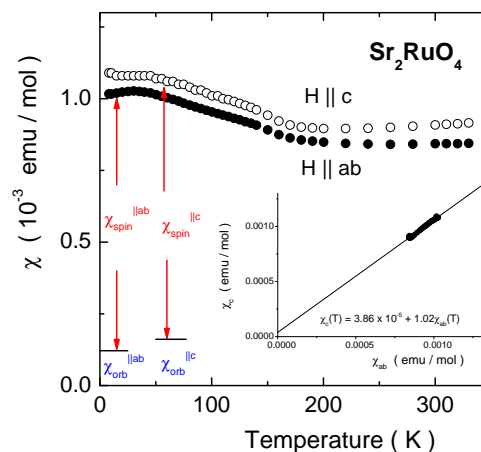


Fig. 3. (Color online) Bulk susceptibility of Sr_2RuO_4 (Refs. 62 and 63) illustrating the spin and orbital contributions (see text for details).

variant through T_c instead. The same measurement was done in field as small as 55 mT confirming the invariance of the spin susceptibility. The occurrence of the superconductivity in the field was confirmed by the measurements of the Meissner signal as well as $1/T_1$ of Ru using the identical set up of the Knight-shift measurements, as shown in Fig. 5(b). Note that the Knight-shift spectra were obtained within 100 μs after the RF pulse with the total duration of 100 μs . In contrast,

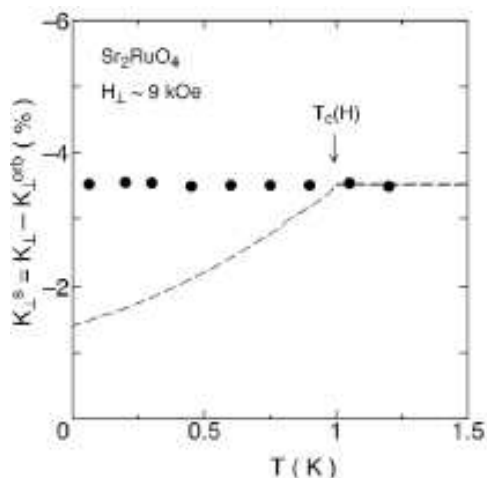


Fig. 4. Knight shift of ^{99}Ru nuclei of Sr_2RuO_4 with the applied field parallel to the basal ab plane (Ref. 62). The spin part $K_s(T)$, after subtracting the temperature-independent orbital part K_{orb} from the total shift $K(T)$, is plotted.

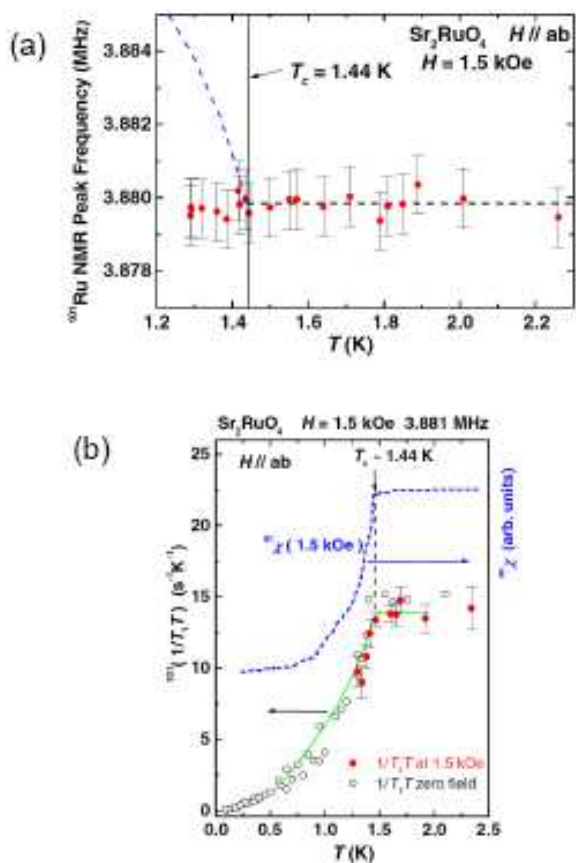


Fig. 5. (Color online) (a) Low-field Knight shift of ^{101}Ru nuclei of Sr_2RuO_4 with the field parallel to the basal ab plane. The Knight shift was obtained from the spectral shift of the NQR frequencies in the presence of a magnetic field. (b) Ac susceptibility χ_{ac} and nuclear spin-lattice relaxation rate $1/T_1$ obtained in the identical setup as used for Fig. 5(a). Taken from Ref. 63.

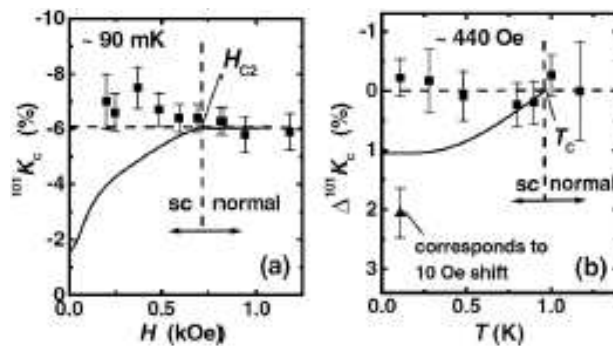


Fig. 6. ^{101}Ru Knight shift $^{101}K_c$ of Sr_2RuO_4 (a) at 90 mT for $H \parallel c$ as small as 20 mT and (b) at various temperatures at 44 mT (Ref. 64). One can see in (a) that the orbital contribution to K_c is -1.6%. In (b) the data point in a triangle is obtained by intentionally varying the external field by 1 mT.

$1/T_1$ was obtained within 100 ms after the pulse. Absence of excessive heating by the RF pulses for the NMR measurements was carefully confirmed by examining the temperature dependence of the spectral peak intensities.

The Knight-shift measurements in magnetic fields perpendicular to the RuO_2 plane (parallel to the c axis), denoted as K_c , were performed in the same way. However the measurements in this direction is difficult for the following two reasons: (1) H_{c2} along the c axis is only 75 mT, 20 times smaller than H_{c2} along the RuO_2 plane; (2) the superconducting fraction with penetrating magnetic field is much more suppressed since the Ginzburg-Landau parameter is as small as 2.6 for $H \parallel c$. Thus, the measurements for $H \parallel c$ were performed with utmost care.

Figure 6(a) shows K_c measured at $T = 90$ mK in the field range from 20 mT to 120 mT, and Fig. 6(b) shows the temperature dependence of K_c measured at 44 mT. In both measurements, no appreciable changes can be detected beyond the experimental error. The solid curves in Figs. 6(a) and 6(b) are conceivable dependences, when the superconducting d -vector is locked along the c axis. Such dependences are inconsistent with experimental results: The spin susceptibility is unchanged also for magnetic fields parallel to the c axis.

Figure 7 summarizes the temperature and field ranges of the Knight-shift measurements performed so far; no appreciable suppression has been detected in any of the measurements. One of the plausible interpretations is that the d -vector orients perpendicular to the external fields greater than 20 mT, irrespective of the field direction.

2.3 Chiral order parameter

The odd parity of the orbital part of the order parameter has been unambiguously demonstrated by phase-sensitive measurements by Nelson *et al.*^{65,66} The critical current of $\text{Au}_{0.5}\text{In}_{0.5}\text{-Sr}_2\text{RuO}_4$ superconducting quantum interference devices (SQUIDs) containing a loop of conventional s -wave superconductor $\text{Au}_{0.5}\text{In}_{0.5}$ and Sr_2RuO_4 prepared on Sr_2RuO_4 single crystals was found to be a maximum for de-

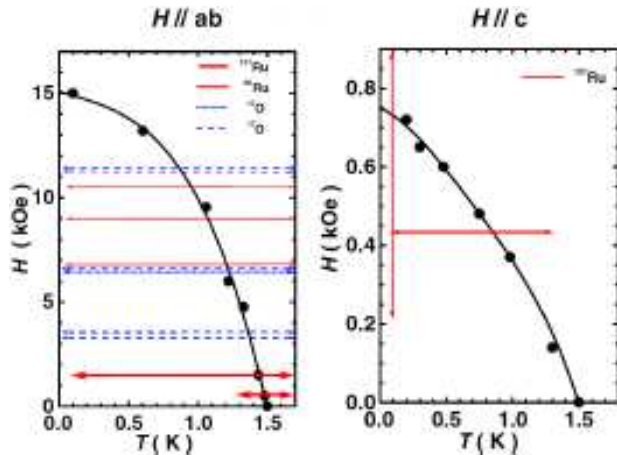


Fig. 7. (Color online) Field-temperature phase diagram of Sr_2RuO_4 summarizing the temperature or field sweeps of the Knight-shift measurements reported so far (Ref. 63).

VICES with junctions on the same side of the crystal and a minimum for devices with junctions on opposite sides, in the limit of zero magnetic flux as shown in Fig. 8. These findings indicate that the phase of the superconducting order parameter in Sr_2RuO_4 changes by π under inversion. This result verifies the odd-parity pairing symmetry corresponding to the formation of spin-triplet Cooper pairs in Sr_2RuO_4 .

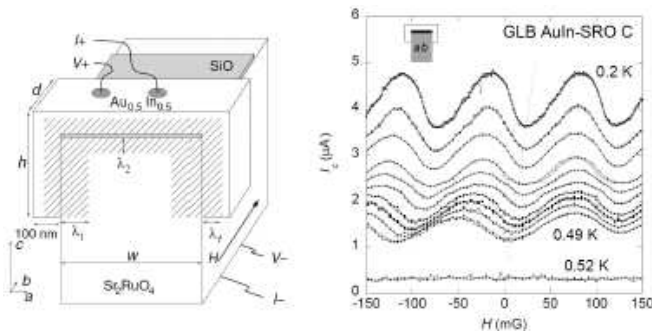


Fig. 8. A π -junction SQUID consisting of $\text{Au}_{0.5}\text{In}_{0.5}$ and Sr_2RuO_4 .⁶⁵ The minimum of its critical current extrapolates to zero towards the superconducting T_c of an s -wave superconductor $\text{Au}_{0.5}\text{In}_{0.5}$, where the induced flux due to the asymmetry of the SQUID is minimized.

Among the candidate odd-parity spin-triplet pairing states listed in Table IV, the Γ_5 state with the orbital order parameter $\Delta(\mathbf{k}) = \Delta_0(k_x \pm ik_y)$ is the so-called “chiral superconducting state”, which is accompanied by the broken time-reversal symmetry (TRS). The term “chiral” is used for the TRS broken state associated with the orbital part of the wave function. The TRS breaking was first demonstrated by the emergence of internal magnetic fields observed in the muon spin resonance experiments.⁴⁸ Since the specific heat demonstrates no residual density of states (DOS), the broken TRS

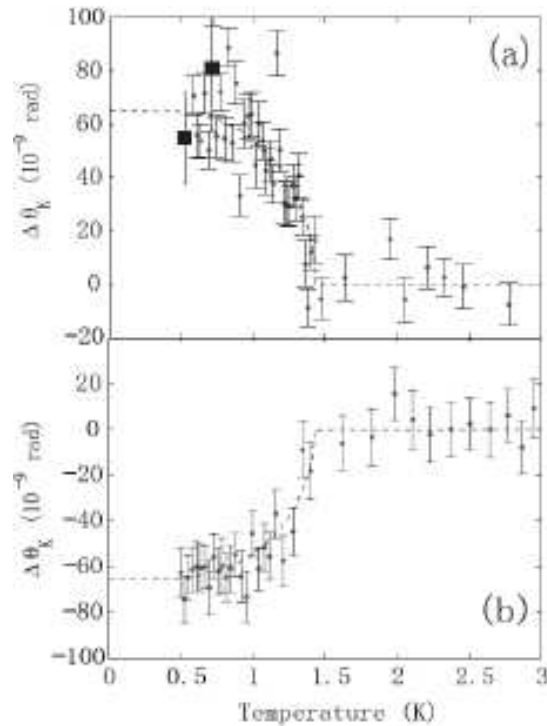


Fig. 9. Rotation angle $\Delta\theta_K$ of the reflected light from the surface of a Sr_2RuO_4 crystal due to magneto-optic Kerr effect (MOKE). The change of about 60 nrad below T_c is attributed to the broken time-reversal symmetry of chiral superconductivity. The sign of $\Delta\theta_K$ can be manipulated by the direction of the external field applied before the measurements, interpreted as the alignment of chiral superconducting domains. From Xia *et al.* (2008).⁶⁸

state associated with the spin part, the so-called “non-unitary state”, is unlikely realized in Sr_2RuO_4 at least under zero magnetic field.

An important progress has been made by the development of ultra-high sensitive magneto-optic Kerr effect (MOKE) apparatus based on a Sagnac interferometer.⁶⁷ The rotation of the polarization plane of the reflected light below T_c shown in Fig. 9 indicates the broken TRS in the superconducting Sr_2RuO_4 .⁶⁸ It is shown that the Kerr signal does not couple strongly with the vortices and that the sign of the Kerr signal is reversed by the application of the field over about 5 mT before the measurements under zero-field are performed. The latter is attributed to the need for training the chiral domains, i.e., enlarging the size of the chiral domain having the same sign of the orbital angular momentum of the Cooper pairs as the external field. Considering the size of the focused laser light used, the trained chiral domain size is estimated to be on the order of a few micrometers. It is worth mentioning that the new technique of MOKE experiments has successfully been applied to investigate broken TRS associated with the inverse proximity effect in the bilayer films consisting of an s -wave superconductor and a ferromagnet.⁶⁹

The MOKE measurements for Sr_2RuO_4 stimulated a number of theoretical investigations.⁷⁰⁻⁷³ In general, the Kerr

rotation angle is expressed in terms of the ac Hall conductivity $\sigma_{xy}(\omega)$, i.e., the off-diagonal part of the ac conductivity tensor. Using appropriate parameters for Sr_2RuO_4 , Yakovenko evaluated the Kerr rotation angle $\Delta\theta_K$ for the chiral p -wave pairing state, and obtained $\Delta\theta_K \approx 230$ nrad.⁷⁰ Goryo presented a mechanism of impurity-induced Kerr rotation. He calculated the Hall conductivity within the low-order expansion in the impurity strength, and found that the leading contribution is given by similar diagrams to the skew-scattering diagrams in the extrinsic anomalous Hall effect. In this impurity-induced mechanism, the MOKE would be suppressed or would be zero for any unitary pairing states other than the chiral pairing state. The rotation angle $\Delta\theta_K$ is evaluated to be about 30 nrad for a realistic impurity mean distance $\ell = 5000$ Å, in agreement with the experimental values.⁷¹ These studies on MOKE suggest that the chiral pairing state is realized in Sr_2RuO_4 .

The chiral superconducting state of Sr_2RuO_4 is supported by a number of experiments, including μSR , Kerr effect, and Josephson effect. The chirality, or the TRS breaking in the orbital wave function, is believed to originate from the $k_x \pm ik_y$ wave function associated with the orbital angular momentum $L_z = 1$ of Cooper pairs. In the bulk of Sr_2RuO_4 crystals, it is expected that domain structures of superconducting regions with opposite chirality form. Strong evidence for the presence of such order parameter domains as well as for the domain wall motion were obtained through anomalous behavior of diffraction patterns of Josephson junctions on single faces of the crystals by Kidwingira *et al.*⁷⁴ The observed telegraph noise in the critical current as a function of magnetic field or time, responsible also for hysteresis observed in field sweeps of the critical current, is attributable to transitions between the chiral states of a domain or the motion of domain walls separating them. Examining the modulation envelopes the data, they estimated average domain width of ~ 1 μm . The presence of such domains confirms the broken time-reversal symmetry nature of the superconducting pairing state in Sr_2RuO_4 .

At a boundary of a chiral superconducting mono-domain, net superconducting edge current is expected within a healing length proportional to the superconducting coherence length. However, this edge current is expected to be screened by the Meissner current extending to the penetration depth from the edge. Since the Ginzburg-Landau parameter is $\kappa = 2.6$, this cancellation must be rather significant. Nevertheless, within the parameters of Sr_2RuO_4 , it is expected that the net magnetic field due to chiral edge current is as large as 1 mT. On the cleaved surface of a single crystal of Sr_2RuO_4 , it is expected that the chiral edge current exists at the bulk edge as well as along the boundaries of $k_x + ik_y$ ($L_z = +1$) and $k_x - ik_y$ ($L_z = -1$) domains.

Aiming at the direct observation of the magnetic field due to the chiral edge current, measurements of scanning SQUID microscope were performed.^{75,76} In both experiments, spontaneous magnetic field was not observed at the bulk boundaries or as an internal pattern suggesting the presence of chiral domain boundaries. After various domain configurations are considered, it is concluded that for the domain size of 2

microns or greater, the magnitude of the magnetic field has to be less than 1% of that expected. Another approach in search for the chiral edge current was taken by a torque magnetometry on a micron-size Sr_2RuO_4 ring; but the result indicated no edge current of the expected magnitude.⁷⁷

We note that Dolocan *et al.* also made direct imaging of magnetic flux structures using a scanning micro-SQUID force microscope, anticipating preferential penetration as well as pinning of vortices along the domain walls.⁷⁸ They observed that as field parallel to the c -axis is increased, individual vortices coalesce and form flux domains. These observations imply the existence of a mechanism for bringing vortices together overcoming the conventional repulsive vortex-vortex interaction. Simulation study of the magnetization process was performed by Ichioka *et al.* for the multidomain state in a chiral p -wave superconductor, using the time-dependent Ginzburg-Landau theory.⁷⁹ They derived a vortex sheet structure forming along a domain wall, and at higher fields the motion of the domain walls so that the unstable domains shrink to vanish. Therefore, the single domain structure would be realized at higher fields.

To explain the absence of magnetic field associated with the edge current, some scenarios have been proposed. Raghu *et al.* proposed an alternative triplet pairing state,⁸⁰ focusing on the hidden quasi-one-dimensional character of the xz and yz bands and the interplay between spin and charge fluctuations on these bands. They obtained a superconducting state without robust chiral edge modes along the boundary, thereby explaining the absence of experimentally detectable edge currents. Based on the Coulomb interaction mechanism presented in § 3, Tada *et al.* showed that the TRS can be restored near the (001) surface because of a Rashba-type spin-orbit interaction.⁸¹ They suggested that such pairing state at the interface is a promising candidate for the recently proposed time-reversal invariant topological superconductivity carrying helical edge current.^{82,83} The surface states they propose naturally lead to cancelled charge current without magnetic field around the edge, although the authors did not explicitly mention a relation to the above experimental results.

These null results for edge currents may also be related to a long-standing profound question concerning the size of the “intrinsic angular momentum” of chiral p -wave superfluid. The chiral edge current originates from a topological property of the bulk and is related to the angular momentum of Cooper pairs.⁸⁴ In a superconductor, Meissner screening current is spontaneously generated in response to the topological edge current. For $^3\text{He-A}$ phase with $\Delta(\mathbf{k}) = \Delta_A(k_x \pm ik_y)$, the expected topological edge mass current has never been observed. The magnitude of the mass current depends on the magnitude of the total angular momentum $\langle L \rangle = (N\hbar/2)(\Delta/E_F)^\alpha$. Depending on whether all the fermions contribute their pair angular momenta or only those in the interaction shell contribute them, the value of α varies as $\alpha = 0, 1$ or 2 . As Leggett notes, this problem “is more than 30 years old and still has apparently not attained a universally agreed resolution.”⁴⁰ The estimated magnitude of the chiral edge charge

current in Sr_2RuO_4 has been largely based on the assumption of $\alpha = 0$, but a reduction factor with $(\Delta/E_F) \sim 10^{-3}$ may have to be included.

2.4 Superconducting gap structure

At the time when the previous review by Mackenzie and Maeno was written, the main issue concerning the gap structure was apparent controversy between the observed low-lying quasi-particle excitations and the predicted fully-gapped state. The former was deduced from the T -linear electronic specific heat coefficient⁸⁵ $C/T \sim T$ and the T -cubed nuclear-spin relaxation rate⁸⁶ $1/T_1 \sim T^3$, as well as from the thermal conductivity,^{87,88} penetration-depth,⁸⁹ and ultrasound attenuation.⁹⁰ The anticipation of the full gap is a consequence of the spin-triplet pairing state on the quasi-two dimensional Fermi surface in the tetragonal symmetry, $\mathbf{d}(\mathbf{k}) = \hat{z}\Delta_0(k_x + ik_y)$ with the isotropic full gap $|\Delta(k_x, k_y)| = \Delta_0$. It was then recognized that multiband effects are important: a large superconducting gap corresponding to T_c opens up on the “active” γ Fermi surface derived mainly from the d_{xy} orbitals of the Ru-4d electrons and having 57% of the total electronic DOS, while the “passive” α and β Fermi surfaces derived mainly from the d_{yz} and d_{zx} orbitals host a gap substantially smaller compared with the energy scale of T_c . The plateau in C/T with increasing $H_{\parallel ab}$ is ascribable to the presence of the small gap in the passive bands with the DOS amounting to 43%. Moreover, nearly-zero gap is expected for these passive bands. At the same time, various models have also been proposed which contain “horizontal” line nodes, with the gap zero at a certain k_z .

A solution to these apparent controversies has been largely given by the specific heat under magnetic fields orientated accurately to the crystalline axes.^{45,91} Before describing details of the superconducting gap structure investigation from these field-angle controlled specific-heat measurements, we first review the theoretically predicted orbital-dependent gap structure. At present, the gap structure semi-quantitatively consistent with the existing experiments is the one predicted by Nomura and Yamada.⁹² As shown in Fig. 19, it consists of a large and anisotropic full-gap on the γ Fermi surface, having a gap minimum along the Γ -M direction (corresponding to the Ru-O [100] direction), and of smaller gaps on the α and β Fermi surfaces, amounting to 1/3 - 1/5 of the gap size on the γ Fermi surface, and having a strong gap minimum accidentally almost zero along the Γ -X (diagonal) directions.

The origins of such “orbital-dependent” gap structure are attributable to the differences in orbital symmetry of each band and in the resulting contribution to the pairing mechanism of each band. Such multiband gap structures with difference in size and anisotropy, introduced in connection with Sr_2RuO_4 ,⁹³ are proven to serve as an important concept also in the superconductivity of other systems such as MgB_2 ⁹⁴ and iron-pnictides.⁹⁵

We next describe somewhat in more detail how the anisotropic gap structure has been deduced from the specific heat.⁴⁵ The quasi-particle spectroscopy using the specific heat

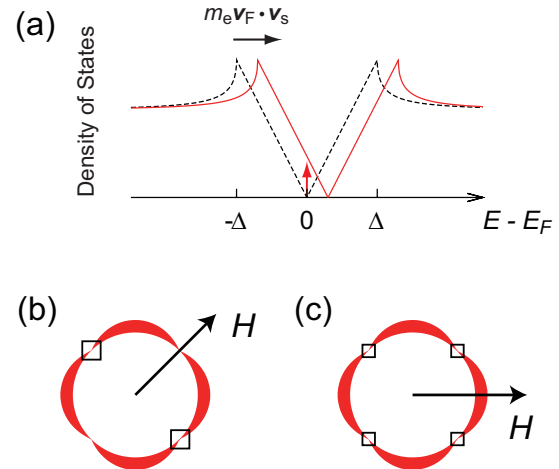


Fig. 10. (a) Volovik effect: the energy shift of a quasi-particle spectrum due to the Doppler effect. Quasi-particle excitations around the nodes or minima of the superconducting gap for the applied magnetic fields parallel to (b) the nodal (or gap minimum) direction and (c) anti-nodal (or gap maximum) direction.

under oriented magnetic fields bases its principle on the so-called Volovik effect.⁹⁶ In the mixed state, the supercurrent velocities around the vortices are perpendicular to the applied field. Since the quasi-particle excitation spectrum is determined with respect to the rest frame of the condensates, the presence of the supercurrents results in the Doppler-shift in the quasi-particle spectrum in the laboratory frame as illustrated in Fig. 10(a): $E(\mathbf{k}) = E_0(\mathbf{k}) + m_e \mathbf{v}_F(\mathbf{k}) \cdot \mathbf{v}_s$, where $E(\mathbf{k})$ and $E_0(\mathbf{k})$ are the quasi-particle spectra in the frames of the laboratory and the condensate, m_e is the electron mass, \mathbf{v}_F and \mathbf{v}_s are the Fermi velocity and the supercurrent velocity, and \mathbf{k} is the quasi-particle wave vector in the laboratory frame. For quasi-two-dimensional superconductors, \mathbf{v}_F is expected to be parallel to \mathbf{k} . As illustrated in Fig. 10(b), this Doppler shift creates field-induced quasi-particle excitations in the regions of the k -vector around gap nodes or gap minima. Such field-induced quasi-particle excitations do not occur for the k -vector parallel to the applied field since \mathbf{v}_F is perpendicular to \mathbf{v}_s . For systems with four line nodes on the two-dimensional Fermi surface, for example, the total quasi-particle excitations are minimized for the field direction along the nodes.⁹⁷ Since the specific heat divided by T or thermal conductivity divided by T is proportional to the quasi-particle DOS at low temperatures, it takes a minimum if the field points to the direction of a nodal or minimum gap position.

An apparatus developed to investigate the field-angle quasi-particle spectra is depicted in Fig. 11.⁹⁸ In this apparatus, the so-called “vector magnet” consisting of split-pair superconducting magnet providing the horizontal field and the solenoid magnet providing the vertical field is placed in the dewar. This dewar rotates horizontally on the platform while the dilution refrigerator inserted in the dewar is fixed. This apparatus allows field alignment with respect to the crystalline

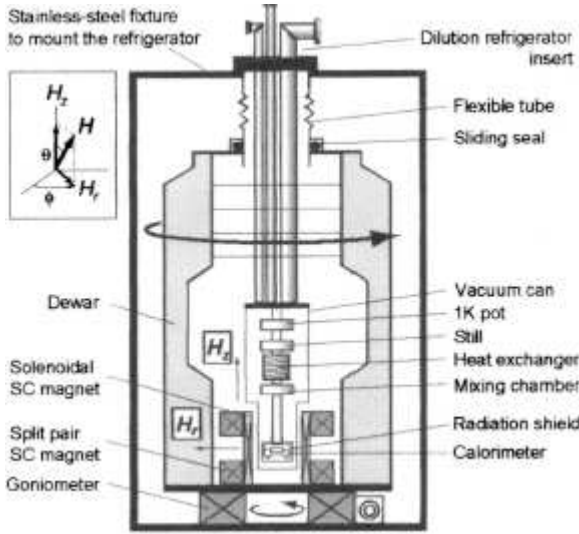


Fig. 11. Apparatus used to measure anisotropic superconducting properties under magnetic fields of accurately and precisely aligned directions. From Deguchi *et al.* (2004).⁹⁸

axes of the sample with high accuracy and precision: the precision in the azimuthal angle of $\Delta\phi \sim 0.001^\circ$ and that of the polar angle of $\Delta\theta \sim 0.01^\circ$ are readily achieved. Because we do not need to rotate the refrigerator, the thermal stability of the measurements is greatly enhanced.

Figure 12 represents C/T with the magnetic field rotating in the basal plane. At relatively high temperatures and near H_{c2} , the four-fold oscillatory component of C/T with minimum along the [110] direction is governed by the anisotropy of H_{c2} with the maximum in that direction below 0.8 K.^{99,100} The data at 0.31 K and 0.12 K clearly exhibit a reversal of the C/T oscillation when the field is reduced away from H_{c2} . In the Doppler shift analysis, the minimum along the [100] direction in this low- H and low- T region indicates that the minimum in the main superconducting gap is in the [100] direction.

Curiously, as the field is reduced below a certain value at the lowest measurement temperature, the oscillatory amplitude in C/T diminishes (Fig. 13), contrary to the expectation of growing relative amplitude for a single-band case. Since the threshold field of diminishing oscillation corresponds well with the exhaustion of the quasi-particle excitations corresponding to the passive α and β bands, it is most naturally explained by the competition of the oscillations between the active and passive bands with opposite gap anisotropies. The specific-heat data under fields tilted from the basal plane assures this interpretation.⁹¹

In addition to the anisotropies due to H_{c2} and nodal gap structure, recent experimental and theoretical studies revealed that the in-plane anisotropy of the specific heat or thermal conductivity in nodal superconductors can change sign, depending on the temperature and field range, due to the vortex scattering effect under rotating magnetic field.¹⁰¹ In fact, such

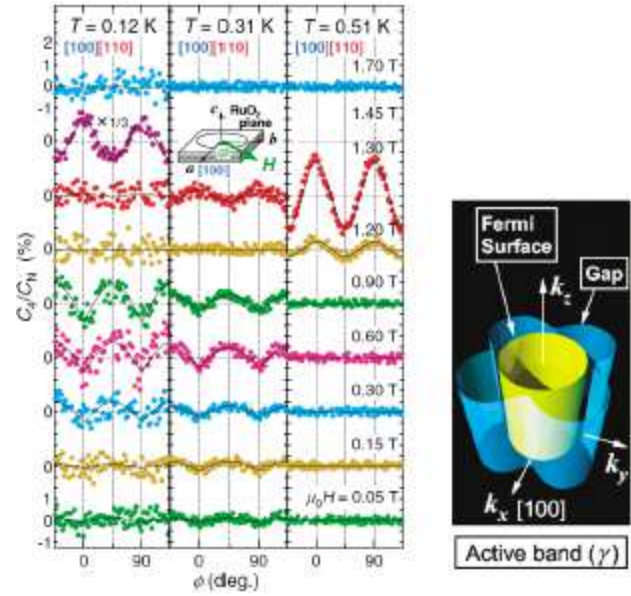


Fig. 12. (Color online) (left) Fourfold oscillation of specific heat of Sr_2RuO_4 under field rotation within the basal plane. Oscillations at high fields are attributable to the anisotropy of H_{c2} .⁹¹ In the low-temperature and low-field region, the oscillation emerges with the opposite phase from the H_{c2} anisotropy. (right) Superconducting gap anisotropy on the active γ band, deduced from the specific-heat oscillations. The gap minima are in the [100] directions. From Deguchi *et al.* (2004).⁴⁵

a sign change was observed at $T \simeq 0.1T_c$ in C/T of the $d_{x^2-y^2}$ -wave superconductor CeCoIn_5 .¹⁰² For Sr_2RuO_4 , the observed large anisotropy at low temperatures probably represents the gap anisotropy of the main band since the measurements were extended to below $0.1T_c$, and the reduction of the anisotropy at the lowest temperature of the measurements is attributed to the multiband effect.

The gap anisotropy consistent with these observations has been predicted by the microscopic theory based on the three-band Hubbard model by Nomura and Yamada.⁹² According to their third-order perturbation theory, described in some detail in § 3, vertex correction terms beyond the second-order spin fluctuation terms play the essential roles for the pairing; the effects of Coulomb repulsion beyond the boson exchange provide the mechanism of unconventional superconductivity. In the heavily doped case as in Sr_2RuO_4 with four electrons with degenerate three bands, a p -wave state is more stable than the d -wave states. Odd parity associated with the p -wave symmetry requires the zero-gap at the symmetry points at the Brillouin-zone (BZ) boundary; naturally the main superconducting gap takes a minimum at the Fermi surface M-point, because it is closest to the BZ symmetry point. The anti-phase anisotropy on the passive bands is also a natural consequence if the antiferromagnetic spin fluctuations due to the nesting of α and β bands are not favorable to the pairing. Thus, the essential superconducting symmetry is given by the chiral p -wave $\mathbf{d}(\mathbf{k}) = \hat{z}\Delta_0(k_x \pm ik_y)$, while the low-lying quasi-particle excitations are attributable to the nearly-zero gap on

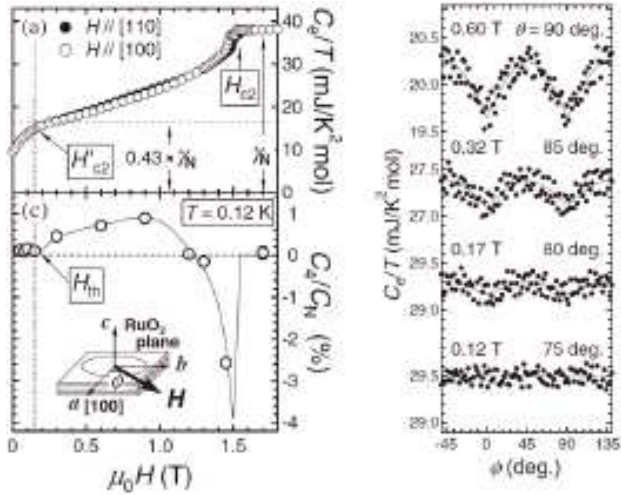


Fig. 13. (left) Correspondence between the quasi-particle excitations under magnetic fields precisely aligned within the basal plane and the magnitudes of the fourfold oscillation amplitude of the specific heat. (right) Dependence on the azimuthal angle ϕ of the specific heat at $T = 0.12$ K for the same reduce field strength of $H/H_{c2}(T)$. The disappearance of the oscillation at lower fields is attributable to the competition between the directions of the superconducting gap anisotropy in the active (γ) and passive (α and β) bands. From Deguchi *et al.* (2004).⁹¹

the passive bands forced by the nesting. We will review other theoretical developments in § 3.

2.5 *d*-vector state

Theoretically, several contributions to determine the direction of the *d*-vector have been considered. The determining mechanisms of the *d*-vector orientation can be divided into two categories.⁴⁴ One is of the “atomic” origin: orbital wave functions of Ru-4*d* and O-2*p* affect the anisotropy of the spins in both the normal and superconducting states. Such atomic spin-orbit interaction (SOI) energy is estimated to be about 50 meV.¹⁰³ (More recently, the SOI energy is calculated to be 90 meV at the Γ point by nonrelativistic band calculations,¹⁰⁴ and to be at least 100 meV based on the comparison between de Haas-van Alphen experiments and relativistic band calculations with local density approximation (LDA).¹⁰⁵) Such SOI energy needs to be considered for electron Cooper pairs, while irrelevant to atomic superfluidity of ³He. In the normal state, the anisotropy of the susceptibility is described as $\chi_c(T) = \chi_0 + 1.02\chi_{ab}(T)$, with the temperature-independent part χ_0 amounting to about 4% of the total susceptibility.⁶¹ The anisotropy of the temperature-dependent part, interpreted as the anisotropy of the spin susceptibility, is only about 2%. Thus in the normal state, there is no strongly preferred orientation of the spins. In the superconducting state, the lifting of the degeneracies of the five possible *d*-vector states due to SOI decides the preferred orientation of the *d*-vector. From the microscopic theories of the pairing reviewed in § 3, the magnitude of the splitting is expected to be four orders of magnitude smaller than SOI itself.

The other mechanism to align the *d*-vector is due to dipolar interaction between the magnetic moments of the spins of a Cooper pair in the chiral state, which favors the *d*-vector parallel to the *L*-vector, namely along the *c* direction. This mechanism dominates the determination of the *d*-vector orientation with respect to the orbital moment in chiral superfluid phase ³He-A. The manipulation of the *d*-vector orientation has been demonstrated by Ahonen *et al.*¹⁰⁶ For ³He confined within narrow parallel plates, the orbital motion is restricted and it is expected that the *L*-vector aligns perpendicular to the plates. The *d*-vector points in the same direction due to the dipolar interaction of about 5 mT. By the application of the in-plane field, the *d*-vector is indeed reoriented.

The first mechanism, atomic SOI associated with the Ru-4*d* orbitals, is incorporated in the microscopic pairing mechanism by Yanase and Ogata,¹⁰³ yielding the *d*-vector pointing in the *c* direction with the anisotropy energy corresponding to 90 mT. Later, Yoshioka and Miyake introduce the importance of the O-2*p* orbitals in the Hubbard model (the *d*-*p* model) and reproduced the $\mathbf{d} \parallel c$ result, but at the same time show that $\mathbf{d} \parallel ab$ becomes more stable if the on-site Coulomb repulsion at the oxygen site, U_{pp} , is comparable to U_{dd} . A more detailed discussion of the atomic SOI will be given in § 3.4. The second mechanism, the spin dipolar interaction within a Cooper pair, favors $\mathbf{d} \parallel c$ with the energy corresponding to 22 mT. Unlike superfluid ³He, the charges of the Cooper-pair electrons lead to the orbital magnetic moment, associated with the orbital angular momentum *L*, which interacts with the spins. Such SOI within a Cooper pair yields the spins orienting parallel to *L*, thus $\mathbf{d} \parallel ab$ by the energy corresponding to 64 mT.¹⁰⁷ Within the five *d*-vector states allowed in the tetragonal crystal symmetry, a *d*-vector in the basal plane may be constructed as a mixing of four of the states. Whether such a state is allowed as the ground state is an issue of current debates. These proposed microscopic mechanisms of orienting the *d*-vector are summarized in Table V.

With these competing mechanisms of comparable magnitudes, it is not easy to predict the *d*-vector orientation theoretically. We note that if the *d*-vector lies in the basal plane, as illustrated in Fig. 1(c), the pinning within the basal plane must be extremely weak because of the tetragonal symmetry. It would then be possible that the *d*-vector orients perpendicular to the external field of any directions; the spin susceptibility is unchanged across T_c , consistent with the NMR Knight-shift observations for both $H \parallel ab$ and $H \parallel c$.

Collective excitations of Cooper pairs manifest the available internal spin and orbital degrees of freedom and give invaluable information of the pairing state. A curious anomaly of the spin-lattice relaxation rate of ¹⁷O under zero magnetic field (NQR) is present in the in-plane oxygen site. Since the principal axis for the oxygen quadrupole moment lies in the basal plane, $1/T_1$ consists of the spin fluctuations of both the in-plane and out-of-plane components. By comparing with the ¹⁰¹Ru NQR relaxation rate, Mukuda *et al.* deduced the anisotropy in $1/T_1$ of ¹⁷O NQR, which exhibits a broad peak below T_c .¹⁰⁹ Miyake recently¹⁰⁷ gives explanation of this be-

Table V. Various microscopic mechanisms of orienting the d -vector and the corresponding stability energies. The stability energies are expressed in units of magnetic field (mT), divided by the Bohr magneton μ_B . *)For $U_{pp} \geq 3t_{dp}$. See § 3.4 for details concerning this condition for the oxygen-site Coulomb interaction U_{pp} and the hopping parameter t_{dp} .

Interaction	Preferred orientation	Stability energy	
Atomic spin-orbit interaction (Ru site)	$\mathbf{d} \parallel \mathbf{L}$ ($\mathbf{d} \parallel c$)	~ 90 mT	(Ref. 153)
Atomic spin-orbit interaction (O site)	$\mathbf{d} \perp \mathbf{L}$ ($\mathbf{d} \parallel ab$)	~ 50 mT *)	(Ref. 160)
Spin-dipolar interaction within a Cooper pair	$\mathbf{d} \parallel \mathbf{L}$	~ 22 mT	(Ref. 108)
Spin-orbit interaction within a Cooper pair	$\mathbf{d} \perp \mathbf{L}$	~ 64 mT	(Ref. 107)
Zeeman interaction ($H \parallel c$)	$\mathbf{d} \perp \mathbf{L}$		
Zeeman interaction ($H \parallel ab$)	$\mathbf{d} \parallel \mathbf{L}$		

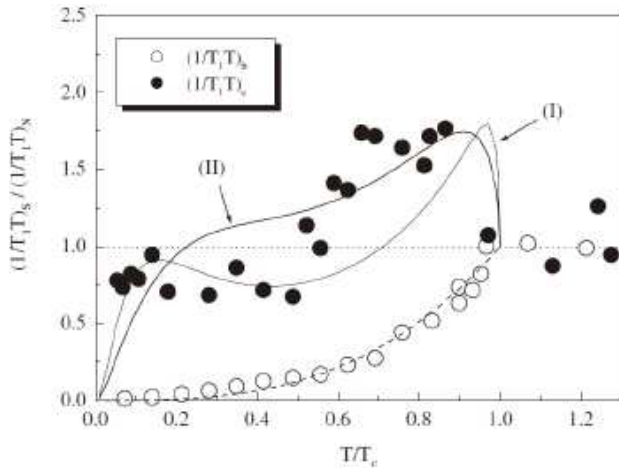


Fig. 14. Spin-lattice relaxation rate of nuclear quadrupole resonance (NQR) of oxygen nuclei. Energy dissipations for both in-plane (open circles) and out-of-plane (closed circles) components in these zero-field data have been deduced. The anomalous enhancement of the out-of-plane absorption is attributed to the collective-mode excitation associated with the d -vector dynamics.¹⁰⁹ The solid curves are theoretical analyses by Miyake.¹⁰⁷

havior as due to the internal Josephson oscillation of the Cooper pairs. As shown in Fig. 14, the oscillation of the d -vector in the basal plane, corresponding to the fluctuation of Cooper-pair spins along the c axis, leads to $1/T_1$ with characteristic two broad peaks below T_c . Although not available at present, ^{17}O NQR signals from the apical oxygen site would give confirming results for this interpretation.

A certain number of theoretical studies on possible collective modes have been done for the spin-triplet pairing state of Sr_2RuO_4 .^{110–116} Among possible collective modes, the most important one is a spin-wave mode which is related to fluctuations of the d -vector direction from its stable direction. If the anisotropy in spin space is neglected, then this mode corresponds to the Goldstone mode accompanied by the symmetry breaking with respect to rotations in spin space and its excitation energy equals zero at the long-wavelength limit $\mathbf{q} = 0$ (because the d -vector rotates freely without any energy cost). In reality, this mode should have an energy gap at

$\mathbf{q} = 0$ (maybe not zero but small gap for Sr_2RuO_4), reflecting the anisotropy of the d -vector. According to the theoretical studies,^{110–116} this mode may be observed experimentally in the in-plane dynamical spin susceptibility, for the chiral pairing state $\mathbf{d}(\mathbf{k}) \propto \hat{z}(k_x \pm ik_y)$. Although such a collective spin excitation has not been observed experimentally, it might be observed in the future, using low-energy neutron scattering or other spin-resonance measurements. Discovery of such a spin collective mode could be strong evidence for the triplet pairing in Sr_2RuO_4 .

3. Pairing by Coulomb repulsion

3.1 Microscopic pairing mechanisms based on Coulomb repulsion

From theoretical points of view, many studies on the triplet pairing mechanism in Sr_2RuO_4 have been performed so far.^{80,117–137} To our knowledge, all of them essentially require unconventional (i.e., non-phonon) mechanisms for explaining the triplet pairing. It is believed that strong electron correlations are much likely to prohibit conventional phonon-mediated pairing in Sr_2RuO_4 . In fact, Sr_2RuO_4 is a typical strongly correlated electron system, as suggested from many experimental and theoretical studies. According to band-structure calculations,^{138,139} Ru- $4d\epsilon$ electrons, which are relatively localized, occupy the states near the Fermi level dominantly, and therefore the electronic properties will be affected significantly by electron correlations. Consistent with this, sizable mass enhancement was observed by quantum oscillation measurements.¹⁴⁰ In addition, it was confirmed that a related compound Ca_2RuO_4 is a Mott insulator.^{141,142}

Here we overview various proposals on the unconventional pairing mechanism for Sr_2RuO_4 . Most of proposed mechanisms can be classified, depending on the microscopic origin of the pairing interaction assumed: (i) ferromagnetic spin fluctuations or paramagnons as in the superfluid ^3He ,^{117–121,137} (ii) anisotropic incommensurate antiferromagnetic spin-fluctuations,^{122–125} (iii) incommensurate charge or orbital fluctuations,¹²⁶ (iv) Hund's-rule coupling among Ru- $4d\epsilon$ electrons,^{127,128} (v) inter-site interaction (including inter-site Coulomb repulsion),^{129,130} and (vi) on-site Coulomb repulsion between Ru- $4d\epsilon$ electrons (particularly among Ru- $4d_{xy}$ electrons).^{131–134} At a first glance, (i) may

seem the most plausible, since Sr_2RuO_4 has Fermi liquid parameters similar to those of superfluid ^3He and the three-dimensional SrRuO_3 is a ferromagnet.^{46,49} However, neutron scattering experiments revealed that the dominant magnetic correlation in Sr_2RuO_4 is incommensurate antiferromagnetic rather than ferromagnetic,¹⁴³ reflecting the nesting character between the α and β Fermi surfaces.^{118,144} In (ii), this incommensurate fluctuation is assumed to be much anisotropic: $\chi_c(\mathbf{Q})/\chi_{ab}(\mathbf{Q}) > 4 - 7$ (\mathbf{Q} is the incommensurate nesting vector).^{122,124} Qualitatively, such anisotropy is indeed consistent with an NMR measurement⁶² and theoretical calculation,¹⁴⁵ but seems too large ($\chi_c(\mathbf{Q})/\chi_{ab}(\mathbf{Q}) \approx 3$ in the NMR experiment). In (iii), incommensurate charge fluctuations due to the nesting between the α and β bands mediate the triplet pairing. In this mechanism, inter-orbital Coulomb interaction should be larger than the intra-orbital Coulomb repulsion somehow.¹²⁶ In the scenarios (ii) and (iii), the pairing interaction will become the strongest on the α and β bands rather than on the main band γ , and therefore the α and β bands will be active ones in pairing transition rather than the γ band, contradicting several experimental results which suggest the dominance of the γ band. In (iv), the Hund's-rule coupling is believed to stabilize the parallel spins of triplet Cooper pairs.^{127,128} However, the Hund's coupling between the local Ru-4d orbitals can stabilize parallel spin states only on each local Ru site, but does not necessarily stabilize them over the superconducting coherence length. It is still unclear whether the Hund's-rule coupling stabilizes spin-triplet pairing rather than spin-singlet pairing in Sr_2RuO_4 or not. In (v), as easily shown, the in-plane inter-site attractive interaction between nearest-neighbor sites induces $\sin k_x$ and $\sin k_y$ -wave pairing.¹²⁹ As for the gap structure in (v), more inter-site couplings between farther sites become necessary to explain the higher-order harmonics of superconducting gap function. If the inter-layer interactions between two sites on adjacent different RuO_2 layers are included, then horizontal line node appears in the superconducting gap.^{129,130,146,147} However, such a horizontal node seems inconsistent with a result of field-oriented specific heat measurement.⁹¹

Recently, Raghu *et al.* presented a two-band calculation for the one-dimensional y_z and x_z bands, in order to explain the absence of edge currents.⁸⁰ For pairing interaction, they used the expression of the second-order perturbation in the on-site intra- and inter-orbital repulsion. This theory seems substantially the same as in (iii). In fact, the obtained momentum dependence of the gap function is very similar to that obtained in the random phase approximation (RPA) calculation of Ref. 126, i.e., the momentum dependence is well approximated by the forms $\Delta_{xz}(\mathbf{k}) \approx \Delta_0 \sin k_x \cos k_y$ and $\Delta_{yz}(\mathbf{k}) \approx \Delta_0 \cos k_x \sin k_y$ in the both theories. The both theories suggest that the triplet pairing becomes more favorable against the singlet pairings, as the inter-orbital repulsion becomes stronger.

At present, we consider that (vi) is the most plausible scenario, in that it adopts only simple assumptions whose origins are microscopically clear or which are consistent with most of

experiments. In the next section we will describe this mechanism in detail.

3.2 Single-band Hubbard model

To describe the above mentioned mechanism (vi), we use weak-coupling approximation, but require nothing except a realistic tight-binding electronic structure and the on-site Coulomb repulsion at each Ru site. First, we consider only the γ band for simplicity, since the γ band takes the major part of the density of states (about 57%) and the heaviest effective mass (14.6 times the bare-electron mass) at the Fermi level.¹⁴⁰ We describe the γ band by a single-band t - t' Hubbard model on a two-dimensional square lattice:¹³¹

$$H = t \sum_{\langle i,j \rangle, \sigma} a_{i\sigma}^\dagger a_{j\sigma} + t' \sum_{\langle i,j \rangle, \sigma} a_{i\sigma}^\dagger a_{j\sigma} + U \sum_i a_{i\uparrow}^\dagger a_{i\downarrow}^\dagger a_{i\downarrow} a_{i\uparrow}, \quad (4)$$

where $a_{i\sigma}$ ($a_{i\sigma}^\dagger$) is the annihilation (creation) operator of an electron with spin σ at Ru site i . Here t and t' are the hopping integrals between nearest and next-nearest neighbor sites respectively, U is the on-site Coulomb integral. We take $t = -1$, $t' = -0.375$, which can reproduce the electronic structure of the γ band approximately. Roughly speaking, since the γ band is constructed mainly from the Ru-4d_{xy} orbitals, the microscopic origin of U is the Coulomb repulsion between the Ru-4d_{xy} electrons. t is estimated to be about 0.25 eV, if the bare bandwidth equals 2 eV. "n.n." ("n.n.n.") means that the summation with respect to i and j is restricted to nearest (next-nearest) neighbor sites. The superconducting transition point is determined by solving the Eliashberg equation:¹³¹

$$\Delta_{\sigma_1\sigma_2}(k) = -\frac{T}{N} \sum_{k'\sigma_3\sigma_4} V_{\sigma_1\sigma_2,\sigma_3\sigma_4}(k, k') |G(k')|^2 \Delta_{\sigma_3\sigma_4}(k'), \quad (5)$$

where $k = (\mathbf{k}, i\omega)$, and $\Delta_{\sigma\sigma'}(k)$ is the superconducting order parameter (in other words, the wave function of Cooper pairs). $G(k)$ is the particle propagator for quasi-particles. $V_{\sigma_1\sigma_2,\sigma_3\sigma_4}(k, k')$ is the pairing interaction, in other words, the scattering amplitude between pairing quasi-particles, where the momenta and spins of the quasi-particles in the initial (final) state are $\mathbf{k}'\sigma_3$ and $-\mathbf{k}'\sigma_4$ ($\mathbf{k}\sigma_1$ and $-\mathbf{k}\sigma_2$). Transition temperature is the highest temperature below which a non-trivial solution $\Delta_{\sigma\sigma'}(k) \neq 0$ appears, and the pairing symmetry is determined by the momentum and spin dependences of the solution $\Delta_{\sigma\sigma'}(k)$.

In the weak-coupling regime, we can evaluate the pairing interaction by perturbation expansion in U :

$$V(k, k') = UV^{(1)}(k, k') + U^2V^{(2)}(k, k') + U^3V^{(3)}(k, k') + \dots \quad (6)$$

Here we have omitted the spin indices for simplicity. The first-order term remains non-zero only in the cases of singlet pairing. This first-order term is independent of momentum and frequency, and is repulsive ($UV^{(1)}(k, k') = U > 0$) in the s -wave channel. This is the reason why the s -wave pairing is generally prohibited in strongly correlated electron systems. Higher-order terms can possess non-trivial momentum de-

pendences, as a result from many-body correlation. The possibility of anisotropic (i.e., non- s -wave) pairing depends on whether this non-trivial momentum dependence is attractive for the corresponding anisotropic pairing channel or not. Thus we turn our attention to the higher-order terms.

The second-order contribution is expressed using the bare susceptibility $\chi_0(q)$ as $U^2 V^{(2)}(k, k') = \pm U^2 \chi_0(k - k')$, where the sign is plus (minus) for singlet (triplet) pairing. In many cases, the bare susceptibility $\chi_0(q)$ captures qualitatively the correct momentum dependence of more precise susceptibility $\chi(q)$ calculated within advanced approximations, e.g., RPA,¹⁴⁸ fluctuation-exchange approximation (FLEX),¹⁴⁹ etc., although the momentum and frequency dependences of the accurate $\chi(q)$ become more enhanced and steeper near magnetic transition points than those of the bare $\chi_0(q)$. In pairing theories based on spin-fluctuation mediation, it is assumed that the pairing interaction can be expressed by the form $V(k, k') \propto \chi(k - k')$, where $\chi(q)$ is calculated by those approximate methods.^{149, 150} Therefore, as far as we discuss qualitative features including the most favorable pairing symmetry, the second-order theory can often predict qualitatively the same results as other methods based on spin-fluctuation mediation. These theories present a clear physical picture that a pair of quasi-particles are formed into a Cooper pair by exchanging elementary excitation ('spin fluctuation' in the present case), where $V(k, k')$ is a function only of the momentum-energy transfer $q = k - k'$, i.e., the momentum and energy of the elementary excitation. Pair-scattering processes due to exchange of elementary excitations are generally represented by such a type of diagrams as in Fig. 15(a).

Next we proceed to the third-order theory. The third-order term $U^3 V^{(3)}(k, k')$ can bring about qualitatively new momentum dependence, as mentioned below. The third-order term consists of RPA-like terms and so-called "vertex-corrected" terms: $U^3 V^{(3)}(k, k') = U^3 V^{(\text{RPA})}(k, k') + U^3 V^{(\text{V.C.})}(k, k')$ (Analytic expressions of the third-order terms are presented in Ref. 131). The RPA-like terms, which are included also within RPA, present qualitatively the same momentum dependence as the second-order term, and are expressed by diagrams of the type (a) of Fig. 15. On the other hand, the vertex-corrected terms do not depend only on $k - k'$, but on both k and k' . Typical examples of third-order vertex-corrected terms are shown in Fig. 15(b). To be regarded as mediated by some kinds of elementary excitations of the system, $V(k, k')$ must be a function only of the momentum and energy ($q = k - k'$) of elementary excitations excited in the intermediate states. Therefore the vertex-corrected terms cannot be regarded as due to exchange processes of any elementary excitations.

Within the third-order perturbation theory, Nomura and Yamada showed that the most probable pairing symmetry on the γ band (Ru- $4d_{xy}$ band) is the spin-triplet p -wave.¹³¹ In Fig. 16, transition temperatures calculated for singlet and triplet pairing states are displayed as a function of U . For the total electron filling of the γ band $n = 1.33$, the highest transition temperature is given by a triplet pairing state, while

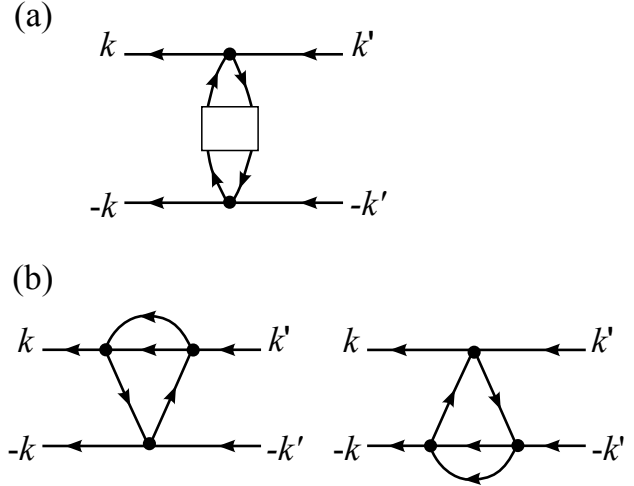


Fig. 15. Diagrammatic representations of typical pair-scattering processes. The filled four-leg vertices and oriented solid lines denote the on-site repulsion U and particle propagator, respectively. (a) General diagrammatic representation of the pair scattering processes which can be regarded as due to exchange of elementary excitations. The rectangle represents arbitrary diagrammatic structure connecting upper and lower parts. Diagrams of this type provide contributions depending only on momentum-energy transfer $q = k - k'$ for the pairing interaction. (b) Typical third-order vertex-corrected terms. Note that these processes are not included in the processes of the above type (a). The diagrams in (b) play an essential role for triplet p -wave pairing.

the singlet $d_{x^2-y^2}$ -wave state becomes favorable toward half filling. Thus, the fact that the electron filling of the γ band is away from half filling is essential for realization of triplet pairing in Sr_2RuO_4 . The momentum dependence of the order parameter $\Delta(k)$ suggests the p -wave symmetry, as shown in Fig. 17 (Only the k_x -type solution $\Delta_x(k)$ is displayed. The k_y -type solution $\Delta_y(k)$ is obtained by $\pi/2$ rotation around the z axis. $\Delta_x(k)$ and $\Delta_y(k)$ transform as k_x and k_y under the D_{4h} symmetry operations, respectively). Here note that the momentum dependence of $\Delta_x(k)$ is not similar to the lowest-order harmonics $\sin k_x$, but seems to contain higher-order harmonics. Although the dominant harmonics is $\sin k_x \cos k_y$, the zero contour of $\Delta_x(k)$ crosses the Fermi circle only at two Fermi surface positions $k_x = 0$. This suggests that line nodes occur at $k_x = 0$ on the realistic cylindrical Fermi surface. However, it should be noted that these line nodes do not cause zero-gap in the energy spectrum, if we also consider $\Delta_y(k)$ of the k_y type as well, because the real energy gap is given by $|\Delta(\mathbf{k})| = [\Delta_x(k)^2 + \Delta_y(k)^2]^{1/2}|_{\omega=0}$ within weak-coupling theories.

In Fig. 18, $V(k, k')$ calculated within the third-order perturbation theory in U is plotted as a function of k for fixed k' . We pay attention to the behavior of $V(k, k')$ near the Fermi surface. We should note that $V(k, k')$ takes low values around $k = k'$ and the maximum value around $k = -k'$. The low values of $V(k, k')$ around $k = k'$ is attributed to the weak ferromagnetic feature of $\chi_0(q)$ (remember that the second-order contribution is expressed by $U^2 V^{(2)}(k, k') = -U^2 \chi_0(k -$

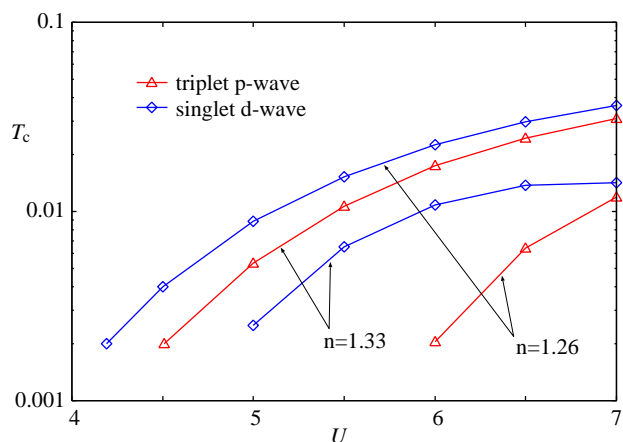


Fig. 16. (Color online) Transition temperature T_c as a function of the on-site repulsion U , calculated by using a single-band Hubbard model for the γ band.¹³¹ n denotes the total electron filling ($n = 1.33$ is the realistic value for the γ band of Sr_2RuO_4). Half filling is $n = 1$.

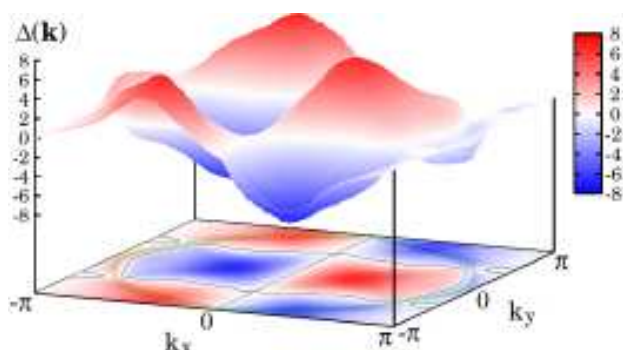


Fig. 17. (Color online) Momentum dependence of the triplet superconducting order parameter $\Delta(k)$ (only the k_x -type). The green circle and gray solid lines on the base plane represent the γ Fermi surface and the zeros of $\Delta(k)$, respectively.

k'). This ferromagnetic feature is due to the fact that the Fermi level is close to the van Hove singularity on the γ band.¹⁴⁴ On the other hand, the high values around $\mathbf{k} = -\mathbf{k}'$ are brought about by the third-order vertex-corrected term $U^3 V^{(V.C.)}(k, k')$. As inferred from the minus sign of the right-hand side of the Eliashberg equation (5), this characteristic momentum dependence of $V(k, k')$ favors sign change of $\Delta(k)$ between \mathbf{k} and $-\mathbf{k}$, and accordingly causes p -wave pairing. It is interesting that the same vertex-corrected terms as shown in Fig. 15(b) cause p -wave pairing also in two-dimensional isotropic repulsive fermion systems in the weak-coupling regime.^{151, 152} At present, we do not know how to draw such a clear and intuitive physical picture on the momentum dependence derived from vertex-corrected terms as that on the momentum dependence due to elementary-excitation mediation. The third-order perturbation calculation has been applied to other unconventional superconductors than Sr_2RuO_4 ,

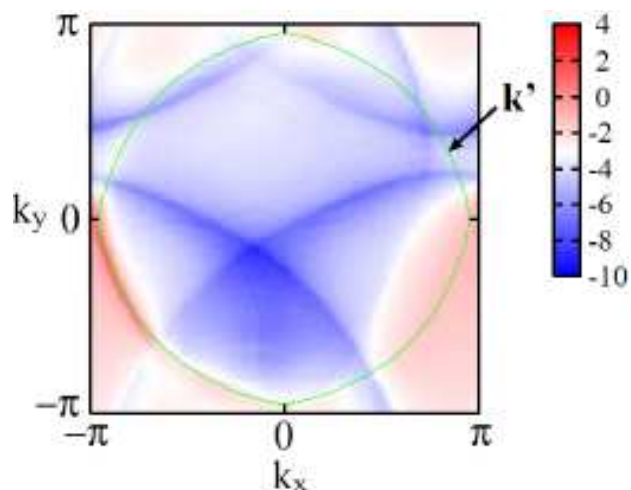


Fig. 18. (Color online) k -dependence of the triplet-pairing interaction $V(k, k')$. k' is fixed at the point indicated by the arrow. The green circle represents the γ Fermi surface. $U = 4$ and $T = 0.002$.

high- T_c cuprates, organics, several heavy-fermion systems, and suggested a plausible pairing symmetry for each of them, so far.¹⁵³ Effects of higher-order contributions are discussed in the Appendix of Ref. 153.

Honerkamp and Salmhofer found the p -wave superconducting phase by applying the one-loop renormalization-group (RG) theory to a similar Hubbard model.^{134, 154} Although the RG analysis does not include one-particle self-energy corrections, it has an advantage that the magnetic, pairing, and other instabilities can be treated on an equal footing. According to their result, the momentum dependence of the effective interaction seems similar to the one obtained within the above third-order perturbation theory, rather than to the one induced by the ferromagnetic spin fluctuation, in spite that the p -wave superconducting phase is adjacent to a ferromagnetic phase. In fact, the RG calculation seems to include the same vertex corrections as the third-order perturbation calculation.

3.3 Extension to three-band model

Nomura and Yamada extended the above single-band calculation to a three-band calculation.^{132, 133} They used a three-band Hubbard model (without SOI) to describe the realistic three-band electronic structure of Sr_2RuO_4 . In the three-band calculation, three components of order parameter, $\Delta_a(k)$ ($a = \alpha, \beta, \gamma$), are required for describing pairing on each band. They determined $\Delta_a(k)$ by solving the Eliashberg equation within the third-order perturbation in the on-site Coulomb integrals. According to their result, the superconducting order parameter takes the maximum value on the γ band. Thus the ‘orbital dependent superconductivity’ initially suggested in Ref. 93 is verified by the microscopic theory. The probable pairing symmetry is reasonably the p -wave again, and the momentum dependence of $\Delta_\gamma(k)$ is almost the same as that by the above single-band calculation for the γ band. Accord-

ing to their three-band calculation, the picture that inter-band proximity¹⁴⁷ induces pairing on the passive α and β bands is indeed valid. In fact, they found that the pairing amplitude $\Delta_\gamma(k)$ on the γ band remains finite and $\Delta_{\alpha,\beta}(k)$ on the passive bands become zero, when the inter-orbital Coulomb interaction is artificially set to zero.

Nomura and Yamada used the three-band solution $\Delta_a(k)$ ($a = \alpha, \beta, \gamma$) for the gap function.^{92,155} If any of the five d -vector states displayed in Table IV is realized, the gap magnitude on each band is calculated by $|\Delta_a(k)| = [\Delta_{a,x}(k)^2 + \Delta_{a,y}(k)^2]^{1/2}|_{\omega=0}$, where $\Delta_{a,x}(k)$ and $\Delta_{a,y}(k)$ are the k_x - and k_y -type solutions on band a , respectively. The gap function predicted by the third-order perturbation theory is presented in Fig. 19. The gap magnitude takes the maximum value on the γ band and the minimum on the β band, reflecting the dominance of the γ band. The calculated result predicts that the superconducting gap should be strongly anisotropic in the basal plane: gap minimum on the γ Fermi surface should exist near the zone boundary, and nearly-zero gap minima on the α and β Fermi surfaces should exist at the diagonal points. The gap minimum on the γ band occurs intrinsically near the zone boundary points $(\pm\pi, 0)$ and $(0, \pm\pi)$, since $\Delta(k) = 0$ holds at the points $(k_x, k_y) = (0, 0), (\pm\pi, 0), (0, \pm\pi)$ and $(\pm\pi, \pm\pi)$ in the Brillouin zone, as straightforwardly verified from odd-parity symmetry and 2π -periodicity of $\Delta(k)$.^{131,156} We should note that the nearly-zero gap minima on the passive α and β surfaces are not a direct result from the symmetry property, in other words, not due to the sign change of the gap function, in contrast to the nodes of $d_{x^2-y^2}$ -wave pairing. The reason why such a strongly anisotropic gap structure appears on the passive α and β bands is that the antiferromagnetic fluctuation due to the nesting between the α and β Fermi surfaces weakens the triplet pairing at these points. Overall, the anisotropy of the main gap structure is quite different from that of the $d_{x^2-y^2}$ symmetry

Nomura and Yamada calculated the specific heat using the above gap function.⁹² They assumed that the momentum dependence of superconducting gap near T_c is preserved down to low temperatures, and simply determine the absolute magnitude of the gap below T_c by the standard BCS gap equation. The calculated result is shown in Fig. 20, and is compared with experimental results.^{85,91} The jump of C/T at T_c is dominated by the contribution from the γ band. Note that, owing to the strongly anisotropic gap structure, the T -linear behavior at low temperatures is reproduced even if the chiral symmetry is assumed. At low temperatures, thermal excitations on the α and β bands, dominantly contribute to the specific heat, due to the nearly-zero gap minima on these passive bands. The same gap function can explain comprehensively the temperature dependences of NMR relaxation rate $(1/T_1T)$,¹⁵⁷ ultrasound attenuation rate, and thermal conductivity.¹⁵⁵

3.4 Role of spin-orbit interaction and d -vector orientation

Electron-electron Coulomb interaction is symmetric under rotations in spin space. Therefore, pairing interaction

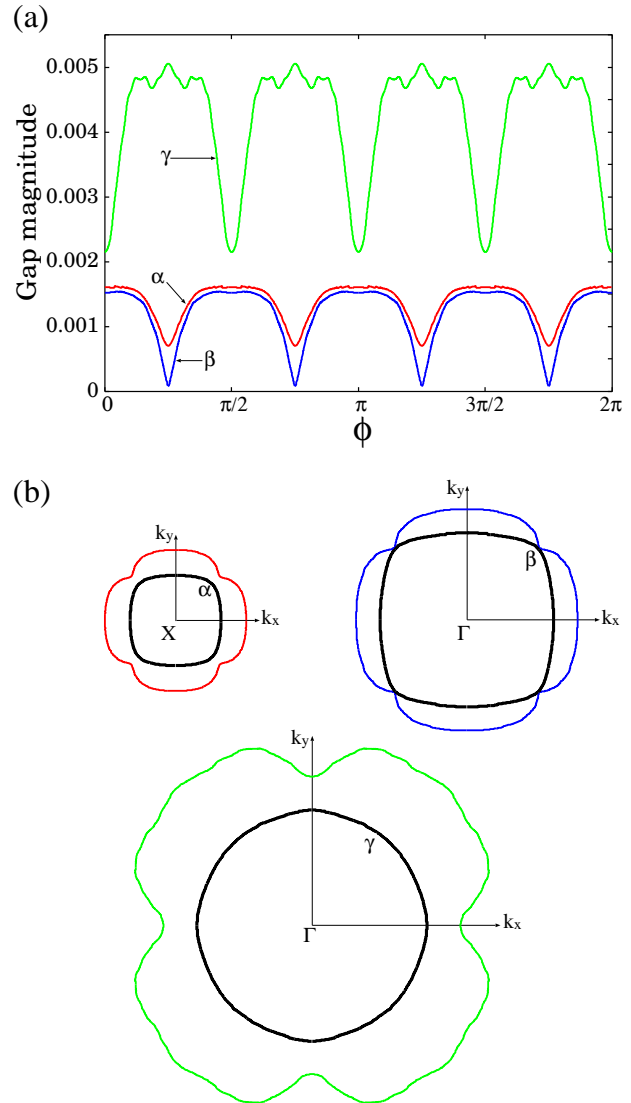


Fig. 19. (Color online) Predicted superconducting gap structure.^{92,155} (a) Gap magnitude on each of the three Fermi surfaces is depicted as a function of the azimuthal angle ϕ around the c axis (the a axis direction corresponds to $\phi = 0$). The unit of energy on the vertical axis is about 0.057 eV. (b) The Fermi surfaces are represented by the solid black circles. The dependence of gap magnitude on in-plane direction is expressed by the distance from the Fermi circle along the direction.

$V(k, k')$ induced only by the Coulomb repulsion does not bring about any anisotropy in spin space, and never lifts the degeneracy of the d -vector states in principle. In § 2.5, three major contributions to the anisotropic energy for the d -vector have been discussed, as summarized in Table V. Among them, we give here a detailed discussion on a leading mechanism of lifting the degeneracy, the “atomic” SOI among the Ru-4d orbitals. This interaction hybridizes different spin and orbital states with each other and causes anisotropy in spin space.^{103,158–160} Although the SOI is believed to be much weak compared with the bandwidth and the Coulomb interac-

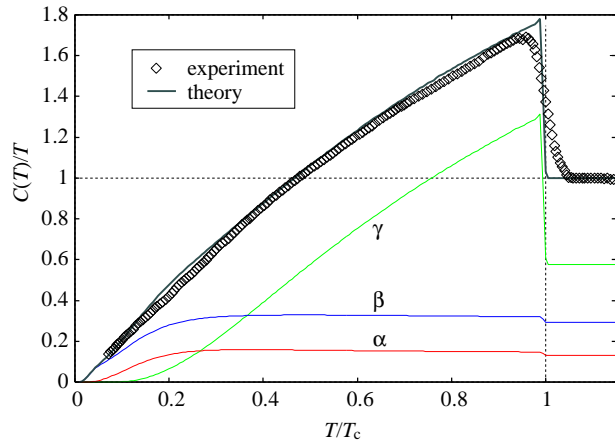


Fig. 20. (Color online) Specific heat C divided by temperature T is displayed as a function of temperature (normalized by the normal-state value).⁹² The solid curves and the diamonds (\diamond) represent the theoretical and experimental data, respectively. Each contribution of the three bands is also depicted separately.

tion for the Ru-4d states (of the order of 100 meV), it plays the essential role for determining the most stable d -vector state. The degenerated d -vector states generally split into five states due to the SOI, as shown in Table IV.

Here we review several microscopic theories including SOI. In the early stage, Ng and Sigrist¹⁵⁸ showed that, under reasonable assumptions, the SOI among the Ru-4d ε orbitals stabilizes the chiral pairing state, where they used $\sin k_x$ and $\sin k_y$ basis functions for the gap function. They used a realistic three-band model including nearest-neighbor ferromagnetic exchange. According to their results, if the pairing interaction is dominant on the γ band, then the chiral state $\mathbf{d}(\mathbf{k}) = \hat{z}\Delta_0(\sin k_x \pm i \sin k_y)$ is reasonably the most stable against the others.

To investigate the possibility of the chiral pairing state in a more microscopic level, Yanase and Ogata included the SOI to perturbation calculation for a three-band Hubbard model.¹⁰³ They treated the SOI within second-order perturbation. For pairing interaction, they performed perturbation expansion in the intra-orbital and inter-orbital Coulomb integrals to third and second order, respectively. The origin of the attractive interaction will be the same as that by Nomura and Yamada, i.e., the third-order vertex-corrected terms with respect to the intra-orbital Coulomb repulsion U . The calculated eigenvalues of the linearized Eliashberg equation are shown in Fig. 21, where note that the d -vector state presenting the larger eigenvalue is the more favorable state. As seen in Fig. 21, the chiral pairing state $\mathbf{d}(\mathbf{k}) \propto \hat{z}(k_x \pm ik_y)$ is expected to be realized at T_c . This is an ESP state with the pair spins in the basal plane.

One might naively consider that the magnetic field necessary to change the direction of the d -vector is estimated from the SOI energy λ via a simple relation $\mu_B B \sim \lambda$. Such estimation is not correct because the anisotropy energy should be

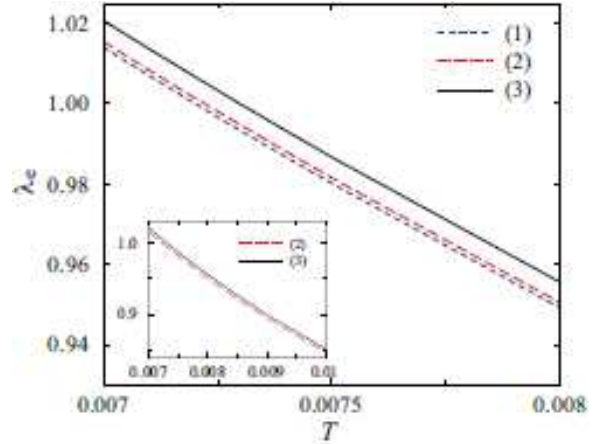


Fig. 21. (Color online) Eigenvalues λ_c as a function of temperature for the five d -vector states:¹⁰³ (1) $\mathbf{d}(\mathbf{k}) \propto \hat{x}k_x \pm \hat{y}k_y$, (2) $\mathbf{d}(\mathbf{k}) \propto \hat{x}k_y \pm \hat{y}k_x$, (3) $\mathbf{d}(\mathbf{k}) \propto \hat{z}(k_x \pm ik_y)$. The inset shows the same in the wide temperature region.

evaluated from the difference in condensation energy among states with different d -vector orientations. This energy should be of the order of $k_B \Delta T_c$, where the difference in transition temperature ΔT_c turns out to be a function of λ/W rather than λ itself, as mentioned below.

Yanase and Ogata showed that realistic value of spin-orbit coupling (about 50 meV) lifts the degeneracy only slightly. This is because the first-order contribution with respect to the spin-orbit coupling vanishes and the symmetry-breaking energy is of the order of $UJ\lambda^2/W^3$ (U : intra-orbital Coulomb repulsion, J : Hund's rule coupling, and W : bandwidth), if the hybridization between different orbitals is completely neglected. According to their estimation, the splitting of T_c between different d -vector states is estimated as $\Delta T_c \sim 0.04T_c$. A very crude estimation using $\mu_B B \sim k_B T_c \cdot (\Delta T_c/T_c)$ leads to 90 mT. Such slight lifting of degeneracy means that the d -vector is not so strongly pinned along the most stable direction and can be rotated easily even by a small magnetic field. In fact, the d -vector direction must be rotated even by a small magnetic field, to be qualitatively consistent with the experimental fact that the NMR Knight shift remains unchanged at T_c under a small magnetic field (20 mT) along the c axis.⁶³

More recently, Yoshioka and Miyake investigated the anisotropy of the d -vector on the basis of the d - p model, including not only the on-site Coulomb repulsion U_{dd} and SOI at each Ru site but the on-site Coulomb repulsion U_{pp} at each O site.¹⁶⁰ They calculated the pairing interaction within the perturbation theory with respect to the on-site Coulomb repulsions U_{dd} and U_{pp} and the SOI λ . They found that, if U_{pp} is assumed to be larger than U_{dd} , the d -vector parallel to the ab plane can be more stable than the one parallel to the c axis, as shown in the phase diagram of Fig. 22. According to their estimation, the splitting of T_c between the $\mathbf{d} \parallel c$ and $\mathbf{d} \perp c$ states due to the SOI is $\Delta T_c \sim 0.022T_c$ for $\lambda = 0.2$

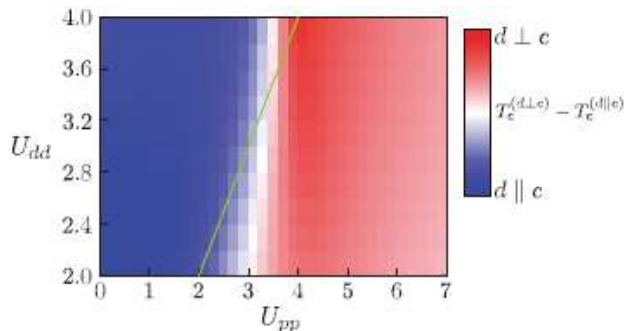


Fig. 22. (Color online) Phase diagram of anisotropy of the d -vector.¹⁶⁰ The stable direction of the d -vector is parallel (perpendicular) to the c axis in the blue (red) region. The green solid line denotes $U_{dd} = U_{pp}$ points.

and $U_{dd} = U_{pp} = 4.0$ (in units of t_{dp} , where t_{dp} is the hopping between nearest-neighbor Ru and O sites). In addition, they showed that the momentum dependence of the order parameter changes from $\sin k_x \cos k_y$ -like to simple $\sin k_x$ -like, around $U_{pp} \sim 3t_{dp}$, as U_{pp} is increased. However, we should note that, according to Table IV, any of d -vector states with $\mathbf{d} \perp c$ do not break TRS in the absence of magnetic fields, and therefore seem incompatible with μ SR results.⁴⁸

At present, the mechanism based on the Coulomb repulsion at Ru site (the main band is γ), incorporated with the atomic SOI at Ru site, reasonably supports the realization of the chiral pairing state. To be consistent with the NMR Knight shift measurement,⁶³ it is necessary to assume that the d -vector along the c axis should be rotated to the ab plane even under a small magnetic field of as small as 20 mT and the Coulomb interaction at oxygen site should not be so large as the d -vector is laid along the ab plane. Of course, the microscopic determination of the most stable d -vector state remains still a subtle issue, because the stabilization energy of the direction of the d -vector is quite small and moreover possibly competing, as mentioned above.

We would like to comment on one of the promising future directions of the microscopic mechanism theory. In all the theories discussed here, simple two-dimensional tight-binding electronic structures are adopted. To proceed to a more precise evaluation of the mechanism and d -vector states, one should use more precise electronic structures based on first-principle calculations. Extension to three-dimensional electronic structures may also prove crucial to resolve some of the important issues, such as suppression of H_{c2} and superconducting multiphase, discussed in § 4.

Recent LDA calculations of the electronic structure and ARPES measurements^{104,161} suggest that the three cylindrical Fermi surfaces cross near the $\langle 110 \rangle$ plane in the absence of the SOI, while actually the crossing is removed by the SOI. According to these results, the orbital character on the Fermi surface varies with k_z , with a tendency of crossing between two-dimensional and one-dimensional bands near $k_z = 0$. Thus we can no longer consider that the γ Fermi surface is con-

structed almost entirely from the xy electrons. Influences of such Fermi surface crossing have not been studied so far, and remain an interesting issue to be investigated in detail.

4. Challenges to the spin-triplet scenario

In this section, we discuss some of the unresolved issues for which explanations in terms of the present spin-triplet p -wave scenario have not been settled. We discuss available theoretical models.

4.1 Suppression of the upper critical field

The H_{c2} of Sr_2RuO_4 is strongly anisotropic, reflecting the quasi-two-dimensional feature of the Fermi surface: 1.5 T for $H \parallel ab$ and 0.075 T for $H \parallel c$. The in-plane H_{c2} anisotropy appears below around 1 K and increases up to 0.04 T. One of the unresolved issues on Sr_2RuO_4 is the temperature dependence of H_{c2} for the field in the ab plane. If the orbital depairing effect dominates in determining H_{c2} , H_{c2} is expected to increase linearly with the initial slope at T_c on cooling and saturates to $-0.7T_c dH_{c2}/dT|_{T=T_c}$ at low temperatures. This behavior is described by the so-called Werthamer-Helfand-Hohenberg (WHH) theory^{162,163} and its extension to p -wave superconductors.^{164,165} Although H_{c2} of Sr_2RuO_4 for $H \parallel c$ exhibits conventional behavior ($H_{c2}(0) = -0.78T_c dH_{c2}/dT|_{T=T_c}$), the in-plane H_{c2} is strongly suppressed at low temperatures ($H_{c2}(0) = -0.42T_c dH_{c2}/dT|_{T=T_c}$).¹⁶⁶

Recently, the Pauli paramagnetic effect was suggested as a possible origin to limit the in-plane H_{c2} of Sr_2RuO_4 .^{167,168} Machida and Ichioka calculated $H_{c2}(\theta)$ as well as the field dependence of the specific heat and magnetization using the Eilenberger equation based on a spherical Fermi surface with the assumption of the paramagnetic depairing effect. Although they suggested that their results reproduced some experimental results, the Pauli effect occurs only for either the singlet pairing state or triplet pairing states with the d -vector locked in a particular direction in the basal plane, which is inconsistent with the results of Knight shift experiments suggesting the triplet pairing with the d -vector state pointing perpendicular to the field in any field direction. The NMR result strongly indicates that Pauli effect is not operative in Sr_2RuO_4 . Qualitatively similar H_{c2} limiting is also known for another spin-triplet superconductor UPT_3 for $H \parallel c$ (Fig. 23),^{169,170} whose origin has not been resolved either. In the field direction in which a strong H_{c2} suppression has been observed, $H \parallel ab$ for Sr_2RuO_4 and $H \parallel c$ for UPT_3 , the d -vector is believed to be perpendicular to the field and thus the Pauli paramagnetic depairing is not anticipated. Thus, the origins of these H_{c2} limitings observed in two plausible spin-triplet superconductors remain challenging issues to be resolved.

In order to clarify the detailed features of the H_{c2} limiting in Sr_2RuO_4 , Kittaka *et al.* performed ac susceptibility measurements with a precise control of the magnetic field direction using a vector magnet system.¹⁷³ They investigated the dependence of H_{c2} on temperature and the angle θ between the magnetic-field direction and the ab plane, as shown

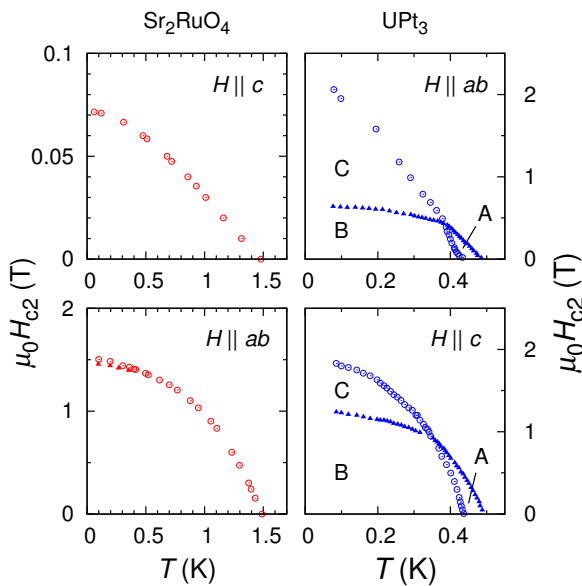


Fig. 23. (Color online) Field-temperature phase diagrams of Sr_2RuO_4 compared with those of UPt_3 . Suppression of H_{c2} of similar magnitude is evident for $H \parallel ab$ in Sr_2RuO_4 and for $H \parallel c$ in UPt_3 . From Deguchi *et al.* (2002, 2004)^{91,171} and Dijk *et al.* (1993).¹⁷²

in Figs. 24(a) and 24(b). It was revealed that the H_{c2} limiting is remarkable only for $|\theta| < 5^\circ$ and remains strong even at relatively high temperatures close to T_c . In the previous study, a clear kink in $H_{c2}(\theta)$ around $\theta = 2^\circ$ was reported from the specific heat measurements at 0.1 K,¹⁷¹ but such a clear feature was not detected at any temperature either by the thermal conductivity¹⁷¹ or recent ac susceptibility^{173,174} (the inset of Fig. 24(b)). It was also revealed that the angular dependence of H_{c2} determined from the ac susceptibility was reproduced with an effective-mass model for an anisotropic three-dimensional superconductor, though the anisotropic ratio needs to vary with temperature.¹⁷³ It is essential to develop a new theory which explains the observed H_{c2} behavior as well as other key experimental results, such as invariance of the Knight shift.

4.2 Superconducting multiphase

A multi-component superconducting order parameter leads to an additional phase transition in magnetic fields. For example, another spin-triplet superconductor UPt_3 is well established to have additional superconducting transition in magnetic fields, resulting from its multi-component order parameter. Also in Sr_2RuO_4 , an additional transition was observed just below H_{c2} at low temperatures below 0.8 K (Fig. 25) by the specific heat,¹⁷¹ dc magnetization,¹⁷⁵ and ac susceptibility.^{174,176} Intriguingly, this additional transition as well as the in-plane H_{c2} anisotropy is suppressed by a slight misalignment of the field from the ab plane; they are observed only for $\theta \lesssim 1^\circ$.¹⁷⁶

Although the mechanism of this superconducting multi-

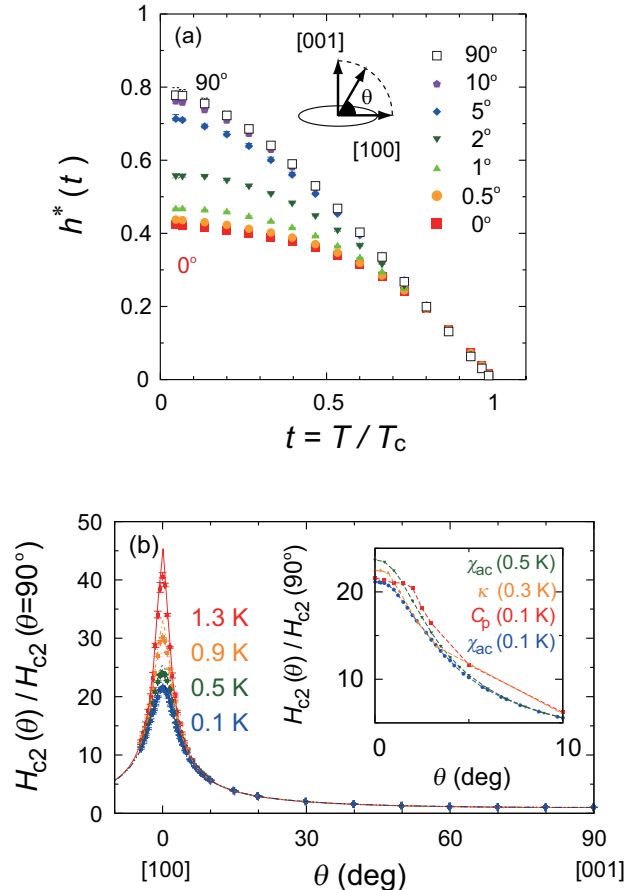


Fig. 24. (Color online) (a) Anisotropy of the upper critical fields H_{c2} of Sr_2RuO_4 . h^* is H_{c2} normalized by the initial slope in the vicinity of T_c . Strong suppression of H_{c2} occurs for the polar angle only within a few degrees from the basal plane. (b) Field-angle θ dependence of H_{c2} normalized by $H_{c2}(\theta = 90^\circ)$. The H_{c2} suppression at $\theta = 0^\circ$ is evident even at relatively high temperatures. From Kittaka *et al.* (2009).¹⁷³ The inset compares the $H_{c2}(\theta)$ determined from various experiments.

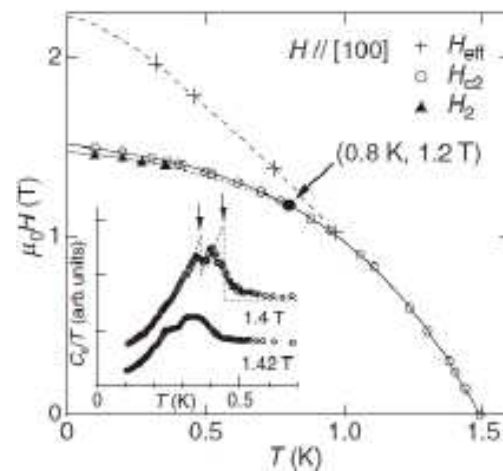


Fig. 25. Field-temperature phase diagram of Sr_2RuO_4 detailing the regions of superconducting double transitions for field accurately aligned within the basal plane. The phase diagram is constructed from the double-peak structure of the temperature dependence of the specific heat. From Deguchi *et al.* (2002).¹⁷¹

phase has been actively discussed, it is still controversial. For a superconductor with $\mathbf{d}(\mathbf{k}) \propto \hat{z}(k_x \pm ik_y)$, if the magnetic field is applied parallel to the x axis, the degeneracy between $\hat{z}k_x$ and $\hat{z}k_y$ is lifted and the transition from $\hat{z}(k_x \pm ik_y)$ to $\hat{z}k_x$ occurs and the non-chiral single-component $\hat{z}k_x$ is expected to become stable near H_{c2} at all temperatures.¹⁷⁷ This additional transition can be easily suppressed by a slight misalignment of the field of only one degree. However, in this theoretical model, large in-plane anisotropy for such additional transition is expected,^{177,178} which is incompatible with the experimental results. Another possibility is the crossover from $\hat{z}k_x$ to the spin-polarized $(\hat{z} - i\hat{y})k_x$ state.¹⁷⁹ In this theory, the transition from $\hat{z}(k_x \pm ik_y)$ to $\hat{z}k_x$ is additionally expected in the region far below H_{c2} . Although a tiny magnetization anomaly far below H_{c2} was reported by Tenya *et al.*,¹⁷⁵ there is no other report which supports the results of the dc magnetization experiment. At present, this scenario is not well established, either. Machida and Ichioka proposed that the second transition is attributed to the FFLO in Pauli limited superconductors.¹⁶⁷ Clearly, there remains a contradiction between the Pauli effect scenario and the results of Knight shift experiments, as written in § 4.1.

5. Novel superconducting phenomena

5.1 Superconductivity in eutectic systems

The intrinsic T_c of pure Sr_2RuO_4 is well established to be 1.5 K.⁴² However, a large diamagnetic signal and the rapid decrease of resistivity with an onset T_c of nearly 3 K are observed in some single crystals of Sr_2RuO_4 . Soon after the discovery of such "3-K phase", it was noticed that the enhanced- T_c superconductivity originates in the Sr_2RuO_4 -Ru eutectic solidification system.¹⁸⁰

The Sr_2RuO_4 -Ru eutectic system is obtained during the single crystal growth of Sr_2RuO_4 with a floating zone technique using Ru self-flux.¹⁸¹ Because volatile RuO_2 evaporates from the surface of melt during the growth, excess Ru needed as a flux tends to solidify in the core region of the crystal rod and coexists with Sr_2RuO_4 , forming a periodic pattern characteristic of eutectic solidification. Figures 26(a) and 26(b) represent polarized optical microscope images of polished surfaces of a eutectic crystal parallel and perpendicular to Ru lamellae, respectively.¹⁸⁰ A number of Ru lamellae (bright area) with typical dimensions of $30 \times 10 \times 1 \mu\text{m}^3$ are embedded in a Sr_2RuO_4 single crystal (dark area). The distance between the nearest lamellae is on typically about $10 \mu\text{m}$. The orientation of Ru lamellae with respect to the crystal axes of Sr_2RuO_4 varies among different crystals and even within the same crystalline rod. Surprisingly, although the values of the unit-cell parameters are different between Sr_2RuO_4 and Ru, it was revealed from transmission electron microscopy (TEM) images that the interface between Ru and Sr_2RuO_4 is atomically sharp, as shown in Figs. 27(a) and 27(b).¹⁸² By contrast, dislocations caused by the lattice mismatch are distributed on a larger scale, as displayed in TEM pictures as dark lines (Figs. 27(c) and 27(d)).

Various experimental results suggest that enhanced- T_c

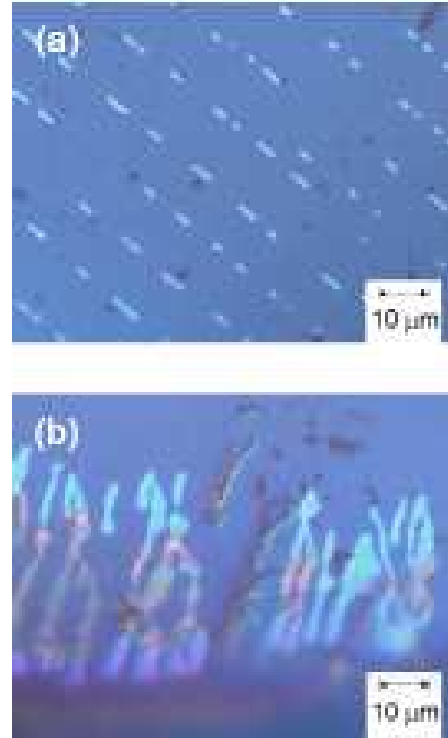


Fig. 26. (Color online) Optical microscope pictures of the surface of a Sr_2RuO_4 -Ru eutectic crystal. Thin Ru metal lamella are embedded in the matrices of Sr_2RuO_4 single crystal. From Maeno *et al.* (1998).¹⁸⁰

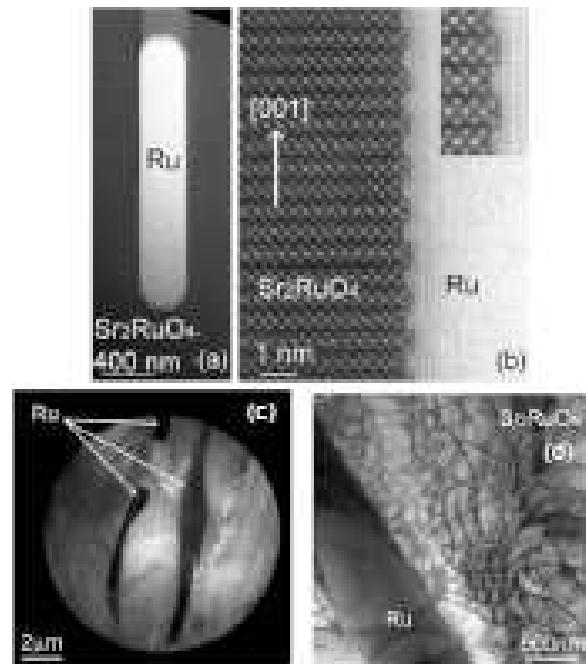


Fig. 27. Transmission electron microscopy images of Sr_2RuO_4 -Ru eutectic crystals. From Ying *et al.* (2009).¹⁸² Note that the dislocation lines in (d) are the results of superposition over many layers.

superconductivity is non-bulk and non- s -wave, occurring in the Sr_2RuO_4 region in the eutectic system. First, a broad transition with a large diamagnetic shielding¹⁸⁰ and a tiny anomaly of the specific heat around 3 K¹⁸³ indicate that the 3-K superconductivity is non-bulk. Second, a zero-bias conductance peak (ZBCP) observed above the bulk T_c of Sr_2RuO_4 in the Sr_2RuO_4 -Ru junctions suggests that non- s -wave superconductivity occurs in the 3-K phase.^{184–186} Third, the anisotropy of H_{c2} clearly depends on the orientation of the crystal axes of Sr_2RuO_4 rather than that of Ru lamellae,^{180, 187} indicating that Sr_2RuO_4 is a stage of enhanced- T_c superconductivity. In the 3-K phase, the formation of Josephson network consisting of inter-lamellar supercurrents is suggested by the zero-voltage current observed at temperatures well above the bulk T_c of Sr_2RuO_4 ¹⁸⁸ and a large diamagnetic shielding with a characteristic response to ac and dc magnetic fields.¹⁸⁹

One of the peculiar features of the 3-K phase is temperature dependence of H_{c2} .¹⁹⁰ Using a definition of H_{c2} as the resistivity inflection point associated with the superconducting transition to the 3-K phase, H_{c2} appears to behave as $(1 - T/T_c)^{0.72}$ for $H \parallel c$ and $(1 - T/T_c)^{0.75}$ for $H \parallel ab$ close to T_c .¹⁸³ In addition, $H_{c2}(T)$ for $H \parallel c$ was revealed to have an upward curvature around 2 K. Such unusual behavior of H_{c2} is explained using a phenomenological theory within the Ginzburg-Landau formalism for an interfacial superconductivity by Sigrist and Monien (S-M).¹⁹¹ They assumed one interface and analyzed with the vector order parameter $\mathbf{d}(\mathbf{k}) = \hat{z}(\eta_x k_x + \eta_y k_y)$, where $(\eta_x, \eta_y) = (1, i)$ is plausible in Sr_2RuO_4 . In the S-M model, it was suggested that the presence of interface parallel to the y axis makes one of the order parameters k_y more stable than the other k_x . By introducing a finite width of the interfacial superconductivity in the S-M model, Matsumoto *et al.* succeeded in reproducing the unusual temperature dependence of H_{c2} more quantitatively.¹⁹² However, the mechanism of the strong in-plane H_{c2} suppression at low temperatures and the origin of the hysteresis behavior observed just below H_{c2} for $H \parallel ab$ remain unresolved.¹⁸⁷

By analyzing the interplay between the chiral p -wave order parameter of Sr_2RuO_4 and the s -wave order parameter of a cylindrical Ru inclusion based on the Ginzburg-Landau formulation, Kaneyasu and Sigrist pointed out that, at a temperature somewhat lower than T_c of Ru (~ 0.49 K), a state emerges with a spontaneous flux distribution around a Ru inclusion.¹⁹³ Moreover, Kaneyasu *et al.* proposed that a discontinuous transition from time-reversal-symmetry-conserving phase to time-reversal-symmetry-breaking phase occurs on cooling at a temperature between 1.5 and 3 K.¹⁹⁴ Their model explains anomalous asymmetric features with respect to the current direction in the current-voltage characteristics observed below 2.3 K¹⁸⁸ as well as the observation of ZBCP below 2.4 K.¹⁸⁵

Recently, hints for clarifying the mechanism of the enhancement of T_c were provided by Kittaka *et al.* from uniaxial pressure experiments.¹⁹⁵ They found that uniaxial pressure along the c axis of only 0.2 GPa induces a broad supercon-

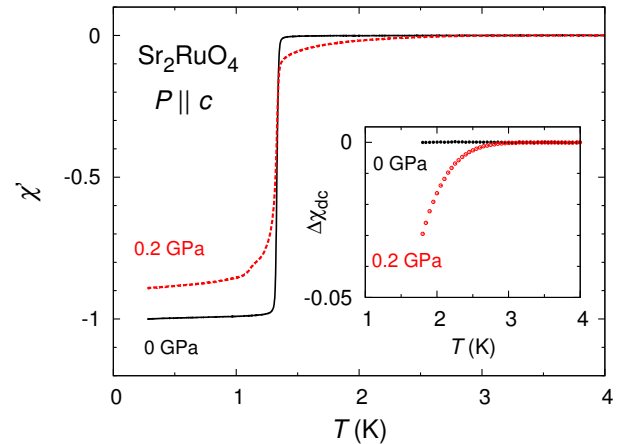


Fig. 28. (Color online) Diamagnetic shielding signals of a pure Sr_2RuO_4 crystal under uniaxial pressure. Evidence for the enhancement of superconducting transition temperature up to 3 K is clearly visible. From Kittaka *et al.* (2010).¹⁹⁵

ducting transition with the onset T_c of about 3.2 K even in a pure, Ru-inclusion-free Sr_2RuO_4 sample with a sharp transition at $T_c = 1.35$ K at ambient pressure. The results of the ac susceptibility measurements are shown in Fig. 28. It was also found that both out-of-plane and in-plane uniaxial pressures largely enhance the magnetic shielding fraction associated with 3-K superconductivity in eutectic samples.^{196, 197} In particular, in-plane uniaxial pressure is much more effective to the enhancement. By contrast, hydrostatic pressure suppresses the bulk T_c of Sr_2RuO_4 ^{198, 199} as well as the shielding fraction associated with 3-K superconductivity.²⁰⁰ These facts strongly indicate that an anisotropic crystal distortion of Sr_2RuO_4 enhances its T_c . Nevertheless, the microscopic origin of this enhancement by anisotropic distortion has not been clarified.

Let us describe another Sr_2RuO_4 -based eutectic system, Sr_2RuO_4 - $\text{Sr}_3\text{Ru}_2\text{O}_7$. Fittipaldi *et al.* found that Sr_2RuO_4 - $\text{Sr}_3\text{Ru}_2\text{O}_7$ eutectic crystals can be grown with a feed rod containing 45% excess Ru with respect to Sr_2RuO_4 under a gas mixture of 10% oxygen and 90% argon with the total pressure of 10 atm.²⁰¹ X-ray diffraction analyses of Sr_2RuO_4 - $\text{Sr}_3\text{Ru}_2\text{O}_7$ eutectic crystals indicate that the directions not only of the c axis but also of the in-plane axes of Sr_2RuO_4 and $\text{Sr}_3\text{Ru}_2\text{O}_7$ are common in the eutectic system.²⁰¹ It was also revealed from TEM images that interfaces parallel to the growth direction (longitudinal direction of a crystalline rod) are sharp and defect-free whereas interfaces perpendicular to the growth direction appear wavy and decorated with Ru precipitates of micron-size.²⁰² In addition, mono-layers of RuO_2 planes with a thickness on the order of nm (very thin Sr_2RuO_4 layer) were revealed to be embedded as stacking faults in the apparent $\text{Sr}_3\text{Ru}_2\text{O}_7$ regions of the eutectic system. Nevertheless, the $\text{Sr}_3\text{Ru}_2\text{O}_7$ domains of the eutectic system have a significantly lower level of impurities, such as $\text{Sr}_4\text{Ru}_3\text{O}_{10}$ ($n = 4$)

and SrRuO_3 ($n = \infty$), compared to $\text{Sr}_3\text{Ru}_2\text{O}_7$ single-phase crystals.²⁰³

In ac susceptibility measurements with an apparent $\text{Sr}_3\text{Ru}_2\text{O}_7$ domain cut from the Sr_2RuO_4 - $\text{Sr}_3\text{Ru}_2\text{O}_7$ eutectic system, multiple superconducting transitions at 1.3 and 1 K were observed.^{204,205} These transitions were revealed to be non-bulk from specific heat measurements and are considered to be attributed to the superconducting transitions of thin Sr_2RuO_4 layers embedded in the $\text{Sr}_3\text{Ru}_2\text{O}_7$ domain as stacking faults. In fact, the anisotropy of H_{c2} of these transitions is the same as that of the bulk Sr_2RuO_4 and H_{c2} for $H \parallel c$ of the transition at 1.3 K (1 K) is compatible with (slightly lower than) that of the bulk Sr_2RuO_4 .^{204,206}

At the early stage, the possibility of the long-range proximity effect in the eutectic system arising from the bulk Sr_2RuO_4 region into $\text{Sr}_3\text{Ru}_2\text{O}_7$ was discussed because finite critical current was observed in a crystal containing a large amount of $\text{Sr}_3\text{Ru}_2\text{O}_7$.²⁰⁷ This finite critical current is probably not due to the long-range proximity effect, but due to the presence of very thin Sr_2RuO_4 -layer inclusions. In fact, T_c of the multiple superconducting transitions is not very sensitive to the electronic state of $\text{Sr}_3\text{Ru}_2\text{O}_7$; although $\text{Sr}_3\text{Ru}_2\text{O}_7$ exhibits ferromagnetism under the uniaxial pressure along the c axis above 0.3 GPa,^{208,209} the onset temperature of the superconducting transition at 1 K is almost invariant or increases slightly under the uniaxial pressure up to 0.4 GPa.²¹⁰ This uniaxial pressure effect is consistent with the scenario that the multiple transitions originate from the embedded thin Sr_2RuO_4 layers.

Recently, Yanase focused on a model of a thin Sr_2RuO_4 layer intercalated in the $\text{Sr}_3\text{Ru}_2\text{O}_7$ domain as a multi-component spin-triplet superconductor with the random spin-orbit coupling.²¹¹ He proposed that the d -vector state in such a Sr_2RuO_4 layer is different from that in the bulk Sr_2RuO_4 and suggested that the d -vector state is locked to be $\mathbf{d}(\mathbf{k}) \propto \hat{x}k_y - \hat{y}k_x$ with time-reversal symmetry.

5.2 Sr_2RuO_4 as a topological superconductor

Recently, quantum phenomena for which underlying topology of wave functions plays fundamental roles are actively investigated with a universal point of view. Topology is a concept and method enabling the classification of shape by continuous deformation. For quantum phenomena, the shape subject to continuous deformation is based on the symmetries and phases of the wave functions. A well-known example of topological quantum phenomena is vortex quantization in a superconductor, for which phase winding associated with real-space topology determines the state. In addition, novel quantum phenomena may emerge in materials for which bulk wave functions themselves have nontrivial topology, characterized by winding numbers defined in momentum space; thus these materials are called the "topological materials". Topological materials include some insulators, superconductors and superfluids and are classified in terms of discrete symmetries of the Hamiltonian as well as the special dimensions.²¹² It has been recognized that states specific to

non-trivial topology and immune to disorder emerge at the edge, i.e., its surface or interface with other materials, according to "bulk-edge" correspondence.²¹³

A chiral p -wave superconductor with the wave function $k_x + ik_y$ is classified among such topological materials and is called a topological superconductor, along with other classes of topological superconductors. For unitary-spin, chiral $k_x + ik_y$ state with broken time-reversal symmetry, the topological invariance is specified by the Chern number.⁸⁴ The chiral edge state discussed in § 2.3 is a consequence of bulk-edge correspondence reflecting the bulk topological properties of a chiral p -wave superconductor. The existence of such chiral edge state has been demonstrated by a recent experiment of quasi-particle tunneling spectroscopy.²¹⁴ In superconductor-insulator-normal metal junctions with Sr_2RuO_4 and Au as shown in Fig. 29, broad humps filling up the gap are observed in the conductance spectra. Compared with the narrow ZBCP associated with the flat-band edge state of $\text{YBa}_2\text{Cu}_3\text{O}_7$ at its (110) interface, the broad conductance peak is a direct manifestation of the chiral edge state characteristic of chiral p -wave superconductivity as shown in Fig. 30. In addition to a number of evidence indicating chiral p -wave symmetry, this confirmation of the chiral edge states reassures that Sr_2RuO_4 is classified as a topological superconductor. Very recently, Sasaki *et al.* found that a bulk superconductor $\text{Cu}_x\text{Bi}_2\text{Se}_3$,^{215,216} derived from a doped topological insulator Bi_2Se_3 , exhibits a similar ZBCP in a "soft" point-contact junction with gold wire attached on the cleaved surface of a $\text{Cu}_x\text{Bi}_2\text{Se}_3$ crystal by silver paste.²¹⁷ After examination of the tunneling spectra in terms of possible superconducting states based on the relatively simple band structure expected for $\text{Cu}_x\text{Bi}_2\text{Se}_3$, they concluded that the observed ZBCP gives crucial evidence for topological superconductivity with odd parity in $\text{Cu}_x\text{Bi}_2\text{Se}_3$.

Such ZBCP emerging at a junction between an unconventional superconductor and a normal metal is a consequence of the density of states due to Andreev bound state.²¹⁸ It has been recognized that such Andreev bound state and the penetration of the pairing amplitude into the normal metal by the proximity effect are intimately related. For an unconventional spin-singlet superconductor, the formation of the Andreev bound state at the junction surface of the unconventional superconductor and the proximity effect are competitive, but it turns out that for a spin-triplet superconductor, they may be constructive, making the proximity effect unusually strong and long-ranged.²¹⁹ As one consequence of such enhancement, it is predicted that due to the proximity penetration of the Andreev bound state into the normal metal, in a T-shaped junction consisting of a spin-triplet superconductor and a normal metal, the density of state of the normal metal increases below T_c of the superconductor.²²⁰

Moreover, it has been recognized that such Andreev bound state can be described in terms of odd-frequency pairing states. In a diffusive normal metal, states other than isotropic s -wave states become difficult to survive. At a junction with a spin-triplet superconductor, therefore, spin-triplet

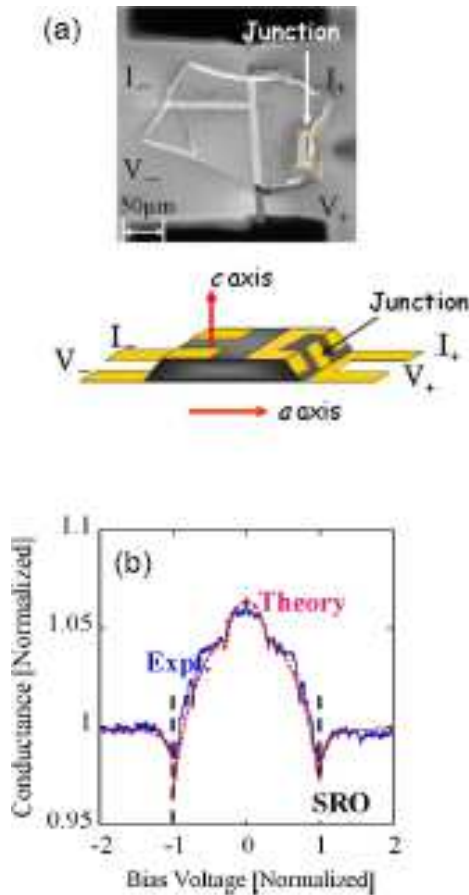


Fig. 29. (Color online) (a) Scanning ion microscopy image of a Sr_2RuO_4 -Au junction fabricated on a SiO_2 substrate and a schematic of the junction structure. (b) Comparison between experimental conductance spectra at 0.55 K (solid lines) and theoretical spectra (dotted lines). From Kashiwaya *et al.* (2011).²¹⁴

s -wave, namely an odd frequency pairing state, is realized.²²¹ Intimate relations among surface bound states, proximity effects, odd-frequency pairing states, and topological edge states are discussed in a recent review by Tanaka, Sato and Nagaosa.²¹³

Concerning the superconducting junctions, it has been recognized that small-size crystal is important to extract the intrinsic unconventional behavior of Sr_2RuO_4 . For a focused ion beam (FIB) fabricated small crystal of $\text{Sr}_2\text{RuO}_4/\text{Ru}$ eutectic, an unusual hysteresis in the current-voltage characteristics has been observed. It was interpreted as due to the motion of the chiral domain walls which alters the critical current.²²²⁻²²⁴

As a novel phenomenon ascribable to real-spatial topology of chiral superconductivity, the critical current of a junction between Sr_2RuO_4 and the s -wave superconductor Pb has been investigated.²²⁵ Pb/Ru/ Sr_2RuO_4 proximity-junctions (Fig. 31) utilizing Ru inclusions in the $\text{Sr}_2\text{RuO}_4/\text{Ru}$ eutectic crystals as a means of achieving a good electrical contact between the two superconductors were fabricated. In such junctions, unusual temperature dependence of the critical current

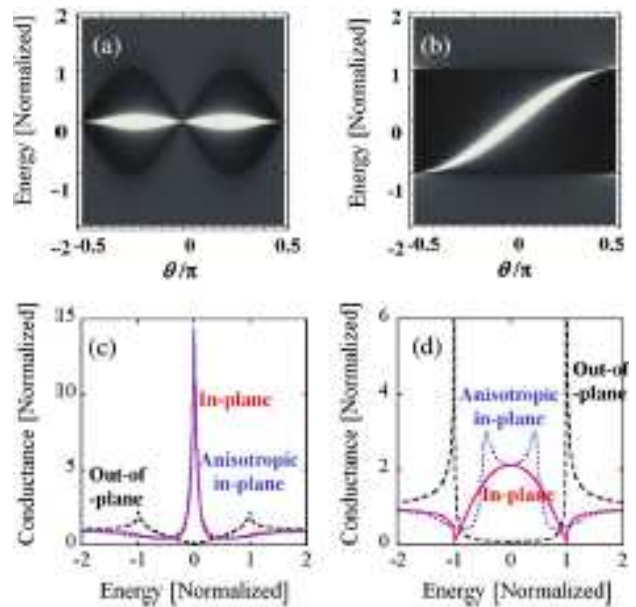


Fig. 30. (Color online) Angle-resolved conductance spectra for (a) d_{xy} -wave superconductors and (b) chiral p -wave superconductors. The vertical axis is the quasiparticle energy normalized by Δ_0 . The brightness represents the magnitude of the junction conductance. Bright regions correspond to the conductance peak originating from Andreev bound states formed at the edge. Conductance spectra for (c) d_{xy} -wave superconductors and (d) chiral p -wave superconductors. From Kashiwaya *et al.* (2011).²¹⁴

is obtained: it increases on cooling from about 3 K but exhibits an unusual sharp drop at the onset of bulk superconductivity of Sr_2RuO_4 at 1.5 K; at lower temperatures the critical current increases again. This unusual behavior is ascribable to topological competition of the phase winding numbers around a Ru inclusion of proximity-induced s -wave superconductivity in Ru and of superconductivity in Sr_2RuO_4 as illustrated in Fig. 32; thus the junction may be called a topological superconducting junction. The phase winding number of Sr_2RuO_4 changes from that of non-chiral p -wave superconductivity of the 3-K phase to the chiral p -wave superconductivity of the bulk Sr_2RuO_4 . We note that a similar phenomenon was reported before in Pb/ Sr_2RuO_4 /Pb junctions with the critical current measured between the two Pb electrodes.²²⁶ In the recent investigation, it is demonstrated that this behavior is essentially obtained in a Pb/Ru/ Sr_2RuO_4 junction configuration with one Pb electrode.

Another remarkable phenomenon associated with real-space topology of superconductivity in Sr_2RuO_4 is emergence of a state related to half-fluxoid state originating from the spin and orbital degrees of freedom. We will describe it in the next section.

5.3 Half-quantum vortices

One of the truly remarkable phenomena expected for spin-triplet states is emergence of the half-quantum vortices (HQV) associated with the magnetic flux just half of the flux

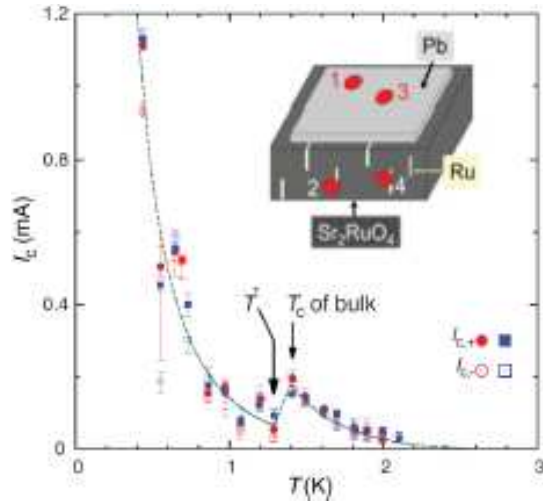


Fig. 31. (Color online) Variation of the critical current I_c with temperature of a Pb/Ru/Sr₂RuO₄ junction. The inset is a schematic of the junction. I_c sharply drops just below T_{c,Sr_2RuO_4} but increases again below a certain temperature designated as T^* . From T. Nakamura *et al.* (2011).²²⁵

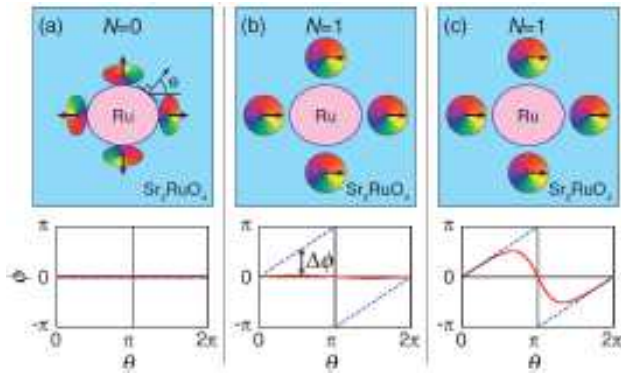


Fig. 32. (Color online) Schematic images of the evolution of the order parameter at the Sr₂RuO₄/Ru interface. In the upper panels, the gradations in the small circles depict the momentum-directional dependence of the superconducting phase ϕ at each spatial position; the arrows denote the momentum direction for which $\phi = 0$. The angle θ is defined as normal to the interface (see (a)). The lower panels represent the superconducting phases $\phi(\theta)$ at the Sr₂RuO₄/Ru interface under no external current. The solid lines represent the phase of s -wave superconductivity in Ru and the broken lines that of p -wave superconductivity in Sr₂RuO₄. (a) $T_{c,Sr_2RuO_4} < T < T_c$: The $k_{||} \pm ik_{\perp}$ state with the winding number $N = 0$ is realized (A' phase), matching with the s -wave order parameter induced in Ru. (b) $T \lesssim T_{c,Sr_2RuO_4}$: Replacement by $k_x \pm ik_y$, the bulk state of Sr₂RuO₄, with $N = \pm 1$ (B phase). (c) $T \ll T_{c,Sr_2RuO_4}$: Increasing interfacial energy enlarges the phase deformation in the s -wave, strengthening the Josephson coupling. From T. Nakamura *et al.* (2011).²²⁵

quantum $\Phi_0 = h/2e$. It was proposed in the context of superfluidity of ³He,^{227,228} but has so far never been confirmed experimentally.²²⁹ In general, flux quantization occurs as a consequence of the single-valuedness of the order parameter around a singularity: either a hole in a superconductor or the vortex core created in the superconductor. Ordinarily, this

single-valuedness is satisfied if the orbital-phase φ variation around a singularity, $\delta\varphi \equiv \oint \nabla\varphi \cdot d\mathbf{s}$, is equal to $2n\pi$ with an integer n . However, for a spin-triplet superconductor of the ESP type, the single-valuedness of the order parameter may also be achieved by a combination of the variations of the spin part as well as the orbital part. To demonstrate this fact, we consider an ESP spin-triplet state $|\Psi\rangle_{\text{ESP}}$ with the spin quantization axis along the x axis, which can be expressed as

$$|\Psi\rangle_{\text{ESP}} = \sqrt{2}\Delta e^{i\varphi} (0, \cos\alpha, \sin\alpha), \quad (7)$$

where the d -vector direction α corresponds to the phase of the spin part as represented in eq. (A.2) in the Appendix. The single-valuedness of this state is satisfied not only if $\delta\varphi = 2n\pi$ and $\delta\alpha = 0$ but also if $\delta\varphi = (2n-1)\pi$ and $\delta\alpha = (2m-1)\pi$, where m is an integer. The latter is an HQV, because only the orbital phase φ couples with the vector potential and thus the magnetic flux. The simplest example with $n = m = 1$ is illustrated in Fig. 33(b), in which the d -vector is represented by an arrow. As we shall see in the Appendix, $|\Psi\rangle_{\text{ESP}}$ can also be expressed as

$$|\Psi\rangle_{\text{ESP}} = \Delta \left(-e^{i\theta_{\uparrow}} |\uparrow\uparrow\rangle_x + e^{i\theta_{\downarrow}} |\downarrow\downarrow\rangle_x \right), \quad (8)$$

where $\theta_{\uparrow} = \varphi - \alpha$ and $\theta_{\downarrow} = \varphi + \alpha$. Thus, an HQV can be interpreted as a vortex for which winding numbers of the components $|\uparrow\uparrow\rangle_x$ and $|\downarrow\downarrow\rangle_x$ are different. Specifically, an HQV with the minimal vorticity, namely with $|2n-1| = |2m-1| = 1$, should be coreless in the sense that one of the two components $|\uparrow\uparrow\rangle_x$ and $|\downarrow\downarrow\rangle_x$ does not have singularity at the center of the HQV, as illustrated in Fig. 33(c).

The HQV involves the rotation of the d -vector and the associated spin currents expressed as $j_s \propto \nabla\alpha$, in which α is the directional angle of the d -vector. Thus the total energy associated with an HQV is

$$E_{\text{HQV}} = C[-\rho_{\text{charge}}(\nabla\varphi)^2 + \rho_{\text{spin}}(\nabla\alpha)^2] \quad (9)$$

with a coefficient C . The charge current associated with an HQV is screened in a distance characterized by the London penetration depth, whereas there is no such screening effect expected for the spin current. To limit the increase of the energy due to spin current, it is anticipated that either a mesoscopic sample size or a closely-separated pair of HQVs is necessary.²³⁰ In the former, when the size of a sample is comparable to the penetration depth, HQVs are similar in energy to full-quantum vortices (FQVs).

In search of an HQV, measurements of magnetic torque of micron-size rings of Sr₂RuO₄ have recently been performed. As shown in Fig. 34, a micrometer-size crystal with a hole drilled by an FIB technique was placed on a silicon cantilever of laser-detected ultra-sensitive torque magnetometer.⁷⁷ The purpose of the central hole is to avoid the complications associated with vortex core production. In such a small sample, the charge supercurrent is non-zero everywhere and it is a fluxoid, given by the sum of flux and kinematic term, rather than a flux, that is quantized to an integer multiple of

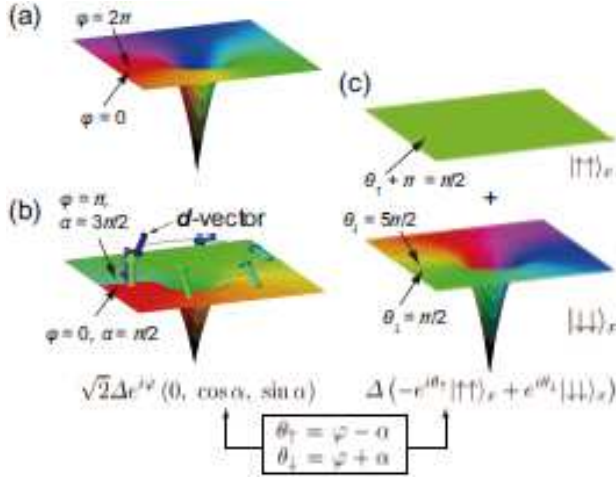


Fig. 33. (Color online) Illustrations of the phases of the superconducting wave function around (a) a full-quantum vortex (FQV) and (b,c) a half-quantized vortex (HQV). As illustrated in (b), a π -rotation of the d -vector direction around an HQV and the π -shift of the orbital wave function recover the single-valuedness of the total wave function. The panel (b) displays an example of an HQV in which the phases of the order parameter change from $(\varphi, \alpha) = (0, \pi/2)$ to $(\pi, 3\pi/2)$. In this example, \mathbf{d} rotates from $\mathbf{d} \parallel \hat{z}$ to $\mathbf{d} \parallel -\hat{z}$. An HQV can be also interpreted as a vortex for which winding numbers of the components $|\uparrow\uparrow\rangle_x$ and $|\downarrow\downarrow\rangle_x$ are different. An example equivalent to the case in (b) is shown in (c). Here, $\theta_\uparrow = \varphi - \alpha$ is constant whereas $\theta_\downarrow = \varphi + \alpha$ changes from $\pi/2$ to $5\pi/2$. Note that the actual phase for $|\uparrow\uparrow\rangle_x$ is $\theta_\uparrow + \pi$ due to the minus sign in the first term in eq. (8).

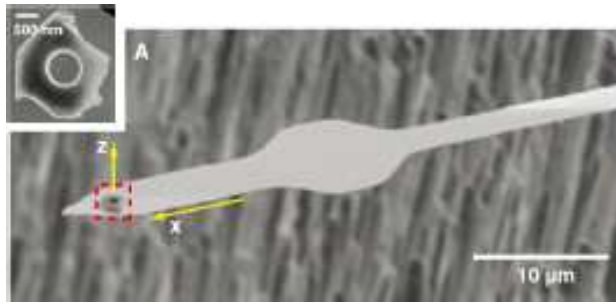


Fig. 34. (Color online) Silicon cantilever used in an ultra-high-sensitivity torque magnetometer with a micron-size crystal ring of Sr_2RuO_4 glued. The Sr_2RuO_4 ring is also shown in the inset. From Jang *et al.* (2011).⁷⁷

flux quantum:

$$\Phi + \frac{m}{e} \oint \mathbf{v}_s \cdot d\mathbf{s} = n\Phi_0 \quad (10)$$

With increasing the magnetic field penetrating the hole, the magnetic moment of the ring is found to decrease uniformly with a negative slope corresponding to the Meissner screening. In addition, a positive jump is observed periodically, corresponding to the full fluxoid quantization. The interval of these jumps is consistent with the fluxoid quantization given by eq. (10).

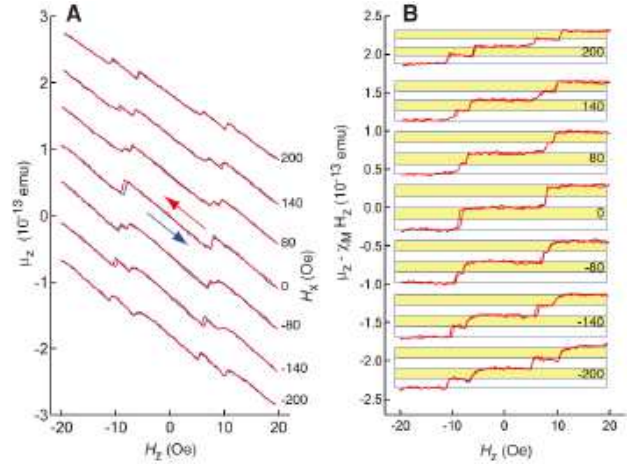


Fig. 35. (Color online) (A) Magnetization of a micron-size ring of a Sr_2RuO_4 crystal under magnetic fields H_z , showing a slope due to Meissner current as well as exhibiting jumps associated with fluxoid quantization. With additional fields perpendicular to the ring axis, the fluxoid jumps split into two. (B) Magnetization of the ring sample after the Meissner shielding contribution has been subtracted. The magnitude of magnetization steps of split jumps is nearly half of that corresponding to a full fluxoid jump. The plateau thus is consistent with a formation of a half-fluxoid state, closely related to the HQV state. From Jang *et al.* (2010).⁷⁷

Unusual jumps between the FQV jumps are observed when additional field is applied perpendicular to the axis of a hole as in Fig. 35. The range of longitudinal field for the stability of the half-fluxoid regions increases nearly proportionally to the perpendicular field. Experimentally, the size of each magnetization jump as well as the magnitude of the longitudinal field is precisely consistent with the half fluxoid expectation. Other possible reasons of the fractional magnetization jumps were examined. For example, penetration of quantized vortices through the side walls may result in the magnetization jumps of varied magnitude. To test this possibility, the perpendicular field is applied to different in-plane direction on the same crystal, but the character of the magnetization jumps remains unchanged: it always occurs as half-fluxoid jumps. The measurements were repeated in several crystals: the HQV feature was not detected in a crystal with the size greater than a few microns, or in NbSe_2 crystals with a comparable anisotropy as Sr_2RuO_4 .

The origin of the necessity of the perpendicular fields has not been fully understood. A semi-quantitatively feasible mechanism is due to “kinematic polarization” proposed by Vakaryuk and Leggett.²³¹ In an HQV state, the orbital winding numbers of the spin-up and spin-down species differ by unity. The associated difference in the kinetic energy due to unbalanced charge current results in the unequal population of each spin species. Application of the field parallel to the ab plane would then lower the spin-polarization energy of an HQV state compared with that of an FQV state. In order to establish the HQV state, other direct measurements of the flux quantization are much desired. In any case, the observations

of half-height flux jumps by Jang *et al.* certainly give additional strong confirmation of the spin-triplet ESP state realized in Sr₂RuO₄.

6. Establishing spin-triplet superconductivity

We have reviewed the current status of our knowledge of unconventional superconductivity in Sr₂RuO₄. From the material perspective, the investigations are greatly helped by the availability of large size, high-quality single crystals: they are chemically-stable, stoichiometric, and having the quasi-particle mean free path more than an order of magnitude greater than the superconducting coherence length. The superconducting eutectic systems containing Sr₂RuO₄ add opportunities to study novel superconducting properties including exotic proximity effects. From the viewpoint of the electronic structure, strongly-correlated multiband Fermi surfaces are relatively simple thanks to the structural simplicity, and the normal state properties are quantitatively well characterized as a Fermi liquid. This allows development of microscopic mechanism theories of unconventional superconductivity based on the realistic multiband Fermi surfaces.

From the extensive NMR studies, the realization of the spin-triplet pairing seems quite certain. Nevertheless, obtaining the complete picture of superconductivity of Sr₂RuO₄ still remains as a challenge. As a promising future direction, we have emphasized the necessity of including spin-orbit interactions in conjunction with three dimensional aspect of the electronic states. Inclusion of these factors may lead to improved interpretations of the mechanism of superconductivity as well as crucial understanding of some of the unresolved issues. To advance further, it is necessary to revisit the superconducting double transitions near H_{c2} as well as the collective-mode excitations observed in the NMR relaxation under zero-magnetic field. Relatively unexplored areas also include the properties of vortex lattice especially with the field parallel to the basal plane.

A new perspective as a “topological superconductor” should also be important. Generation of half-quantum vortices, observation of phenomena associated with chiral edge states, fabrication of superconducting junctions exhibiting novel behavior such as odd-frequency pairing states are some of the promising future directions. Studies using micron-size crystals are proven to be essential to uncover some of these phenomena. At the same time, in order to firmly establish the chiral p -wave state with the two-component order parameter, superconducting properties under symmetry-breaking fields, for example, in-plane uniaxial pressure, may provide useful information.

The extensive efforts to elucidate the superconductivity of Sr₂RuO₄ in all details demonstrate the possible approaches that can be taken to unveil novel behaviors of an unconventional superconductor. In this sense, we hope that this review also serves useful for the studies of other unconventional superconductors.

Acknowledgement

The authors would like to thank M. Sigrist, K. Yamada, A. P. Mackenzie, K. Deguchi, Y. Yanase, S. Kashiyama, Y. Tanaka, Y. Asano, H. Ikeda, H. Yaguchi, A. Kapitulnik, Z. X. Shen, K. Molar, C. Kallin, Y. Liu, K. Miyake, Y. Hasegawa, K. Machida, T. Ishiguro, R. Budakian, D. F. Agterberg, A. J. Leggett, T. M. Rice, A. Vecchione, R. Fittipaldi, Taketomo Nakamura, T. Terashima, I. Vekhter, V. P. Mineev, J. A. Sauls, and J. Goryo for valuable communications. This work was supported by the “Topological Quantum Phenomena” (22103002) and “Heavy Electrons” (20102006, 23102705) Grant-in-Aid for Scientific Research on Innovative Areas, a Grant-in-Aid for the Global COE program “The Next Generation of Physics, Spun from Universality and Emergence”, and Research Activity Start-up (22840013) from the Ministry of Education, Culture, Sports, Science and Technology (MEXT) of Japan and the Japan Society for the Promotion of Science.

Appendix: Two equivalent interpretations of the half-integer quantum vortex

As briefly mentioned in § 5.3, there are two equivalent interpretations of the half-integer quantum vortex (HQV): One is that $(2n - 1)\pi$ phase shift in the orbital part of the order parameter and additional $(2m - 1)\pi$ phase shift in the spin part around an HQV. The other interpretation is a vortex for which winding numbers of the two ESP components are different. In this Appendix, we explain the equivalence of these two interpretations.

First, we write again the definitions of the bases of the d -vector:

$$\begin{aligned}\hat{x} &\equiv |S_x = 0\rangle = \frac{1}{\sqrt{2}} (-|\uparrow\uparrow\rangle_z + |\downarrow\downarrow\rangle_z), \\ \hat{y} &\equiv |S_y = 0\rangle = \frac{i}{\sqrt{2}} (|\uparrow\uparrow\rangle_z + |\downarrow\downarrow\rangle_z), \\ \hat{z} &\equiv |S_z = 0\rangle = \frac{1}{\sqrt{2}} (|\uparrow\downarrow\rangle_z + |\downarrow\uparrow\rangle_z),\end{aligned}$$

where the subscript z in the state vectors indicates that the spin quantization axis is the z axis. If one takes x as the spin quantization axis, an alternative equivalent set is obtained as

$$\begin{aligned}\hat{x} &\equiv |S_x = 0\rangle = \frac{1}{\sqrt{2}} (|\uparrow\downarrow\rangle_x + |\downarrow\uparrow\rangle_x), \\ \hat{y} &\equiv |S_y = 0\rangle = \frac{1}{\sqrt{2}} (-|\uparrow\uparrow\rangle_x + |\downarrow\downarrow\rangle_x), \\ \hat{z} &\equiv |S_z = 0\rangle = \frac{i}{\sqrt{2}} (|\uparrow\uparrow\rangle_x + |\downarrow\downarrow\rangle_x).\end{aligned}$$

Here, we start with a spin-triplet equal-spin pairing (ESP) state $|\Psi\rangle_{\text{ESP}}$ with the quantization axis along x :

$$|\Psi\rangle_{\text{ESP}} = \mathcal{A} \left(-e^{i\theta_\uparrow} |\uparrow\uparrow\rangle_x + e^{i\theta_\downarrow} |\downarrow\downarrow\rangle_x \right). \quad (\text{A}\cdot 1)$$

We note that the minus sign in the first term is just for a convenience that the state with the zero phases $\theta_\uparrow = \theta_\downarrow = 0$ cor-

responds to the \hat{y} state. Then, we can convert them to another set of phases: $\alpha \equiv (\theta_{\downarrow} - \theta_{\uparrow})/2$ and $\varphi \equiv (\theta_{\downarrow} + \theta_{\uparrow})/2$. Using α and φ , $|\Psi\rangle_{\text{ESP}}$ can be expressed as

$$|\Psi\rangle_{\text{ESP}} = \Delta e^{i\varphi} \left(-e^{-i\alpha} |\uparrow\uparrow\rangle_x + e^{i\alpha} |\downarrow\downarrow\rangle_x \right). \quad (\text{A}\cdot 2)$$

This equation can be further modified using the relations $|\uparrow\uparrow\rangle_x = -(\hat{y} + i\hat{z})/\sqrt{2}$ and $|\downarrow\downarrow\rangle_x = (\hat{y} - i\hat{z})/\sqrt{2}$ as

$$\begin{aligned} |\Psi\rangle_{\text{ESP}} &= \frac{\Delta e^{i\varphi}}{\sqrt{2}} \left[(e^{i\alpha} + e^{-i\alpha})\hat{y} + (e^{i\alpha} - e^{-i\alpha})(-i\hat{z}) \right] \\ &= \sqrt{2}\Delta e^{i\varphi} (0, \cos \alpha, \sin \alpha). \end{aligned} \quad (\text{A}\cdot 3)$$

Thus, this relation indicates that φ , the average of the phases of the up- and down-spin components, corresponds to the phase of the orbital part of the order parameter, and that α , the half-difference between θ_{\uparrow} and θ_{\downarrow} , corresponds to the direction of the d -vector in the plane perpendicular to the quantization axis.

When an ordinary full-quantum vortex (FQV) exists, the orbital phase φ must shift by $\pm 2n\pi$ after a circulation around the vortex in order to satisfy the single-valuedness of the wavefunction. According to eq. (A.3), the single-valuedness is also satisfied if the phases α and φ both additionally shift by $\pm\pi$. This is the HQV, because only the shift in the orbital phase φ couples to the vector potential resulting in the magnetic flux of $\Phi_0/2 = h/4e$. As one can see, the π phase shift in α around an HQV corresponds to a rotation of the d -vector by 180° around the quantization axis. These facts are illustrated in Fig. 33(b). In an alternative viewpoint, the phase for the up-spin component $|\uparrow\uparrow\rangle_x$ is $\theta_{\uparrow} = \varphi - \alpha$ and the phase for $|\downarrow\downarrow\rangle_x$ is $\theta_{\downarrow} = \varphi + \alpha$ as shown in eq. (A.2). Thus, the winding numbers of θ_{\uparrow} and θ_{\downarrow} are different around an HQV. A remarkable example is the case that the shifts in α and φ around an HQV are both $\pm\pi$. In such cases, only one of $|\uparrow\uparrow\rangle_x$ and $|\downarrow\downarrow\rangle_x$ exhibits a phase shift of $\pm 2\pi$, whereas the other exhibits zero shift. Thus, one of the two components $|\uparrow\uparrow\rangle_x$ and $|\downarrow\downarrow\rangle_x$ has zero vorticity around an HQV as schematically explained in Fig. 33(c). Such an HQV is ‘‘coreless’’ in a sense that one of the two components has no singularity at the center of the HQV, if it is realized in a simply connected bulk sample.

- 1) J. G. Bednorz and K. A. Müller: Z. Phys. B **64** (1986) 189.
- 2) In Refs. 232 and 233, the term ‘‘unconventional superconductivity’’ is used for superconductivity in which other symmetry than the $U(1)$ -gauge symmetry is additionally broken and consequently the superconducting state does not have the full point symmetry of the crystal lattice, i.e., it does not belong to the identity representation of the crystal point group. However, if we follow this definition, such sign-reversed s -wave superconductivity as recently predicted for iron pnictides^{95,234} is *not* necessarily categorized into ‘unconventional superconductivity’. Therefore, in the present review, we define ‘unconventional superconductivity’ as *superconductivity due to non-phonon (non-BCS) mechanism*, because today researchers adopt tacitly the latter definition rather than the former in most cases, as far as we see. Of course, we consider that these two definitions are consistent with each other for most cases.
- 3) F. Steglich, J. Aarts, C. D. Bredl, W. Lieke, D. Meschede, W. Franz,

- and H. Schäfer: Phys. Rev. Lett. **43** (1979) 1892.
- 4) D. Jérôme, A. Mazaud, M. Ribault, and K. Bechgaard: J. Phys. Lett. **41** (1980) 95.
 - 5) Y. Maeno, H. Hashimoto, K. Yoshida, S. Nishizaki, T. Fujita, J. G. Bednorz, and F. Lichtenberg: Nature (London) **372** (1994) 532.
 - 6) Y. Kamihara, T. Watanabe, M. Hirano, and H. Hosono: J. Am. Chem. Soc. **130** (2008) 3296.
 - 7) J. C. Wheatley: Rev. Mod. Phys. **47** (1975) 415.
 - 8) A. J. Leggett: Rev. Mod. Phys. **47** (1975) 331.
 - 9) G. R. Stewart, Z. Fisk, J. O. Willis, and J. L. Smith: Phys. Rev. Lett. **52** (1984) 679.
 - 10) C. Geibel, S. Thies, D. Kaczorowski, A. Mehner, A. Grauel, B. Seidel, U. Ahlheim, R. Helfrich, K. Petersen, C. D. Bredl, and F. Steglich: Z. Phys. B **83** (1991) 305.
 - 11) K. Ishida, D. Ozaki, T. Kamatsuka, H. Tou, M. Kyogaku, Y. Kitaoka, N. Tateiwa, N. K. Sato, N. Aso, C. Geibel, and F. Steglich: Phys. Rev. Lett. **89** (2002) 037002.
 - 12) M. Kyogaku, Y. Kitaoka, K. Asayama, C. Geibel, C. Schank, and F. Steglich: J. Phys. Soc. Jpn. **62** (1993) 4016.
 - 13) H. Tou, K. Ishida, and Y. Kitaoka: J. Phys. Soc. Jpn. **74** (2005) 1245.
 - 14) S. S. Saxena, P. Agarwal, K. Ahilan, F. M. Grosche, R. K. W. Haselwimmer, M. J. Steiner, E. Pugh, I. R. Walker, S. R. Julian, P. Monthoux, G. G. Lonzarich, A. Huxley, I. Sheikin, D. Braithwaite, and J. Flouquet: Nature (London) **406** (2000) 587.
 - 15) D. Aoki, A. Huxley, E. Ressouche, D. Braithwaite, J. Flouquet, J.-P. Brison, E. Lhotel, and C. Paulsen: Nature (London) **413** (2001) 613.
 - 16) T. Akazawa, H. Hidaka, H. Kotegawa, T. C. Kobayashi, T. Fujiwara, E. Yamamoto, Y. Haga, R. Settai, and Y. Ōnuki: J. Phys. Soc. Jpn. **73** (2004) 3129.
 - 17) N. T. Huy, A. Gasparini, D. E. de Nijs, Y. Huang, J. C. P. Klaasse, T. Gortenmulder, A. de Visser, A. Hamann, T. Görlach, and H. v. Löhneysen: Phys. Rev. Lett. **99** (2007) 067006.
 - 18) H. Tou, Y. Kitaoka, K. Ishida, K. Asayama, N. Kimura, Y. Ōnuki, E. Yamamoto, Y. Haga, and K. Maezawa: Phys. Rev. Lett. **80** (1998) 3129.
 - 19) I. Sheikin, A. Huxley, D. Braithwaite, J. P. Brison, S. Watanabe, K. Miyake, and J. Flouquet: Phys. Rev. B **64** (2001) 220503(R).
 - 20) F. Hardy and A. D. Huxley: Phys. Rev. Lett. **94** (2005) 247006.
 - 21) F. Lévy, I. Sheikin, B. Grenier, and A. D. Huxley: Science **309** (2005) 1343.
 - 22) D. Aoki, T. D. Matsuda, V. Taufour, E. Hassinger, G. Knebel, and J. Flouquet: J. Phys. Soc. Jpn. **78** (2009) 113709.
 - 23) H. Mukuda, T. Ohara, M. Yashima, Y. Kitaoka, R. Settai, Y. Ōnuki, K. M. Itoh, and E. E. Haller: Phys. Rev. Lett. **104** (2010) 017002.
 - 24) M. Nishiyama, Y. Inada, and G.-q. Zheng: Phys. Rev. Lett. **98** (2007) 047002.
 - 25) N. Kimura, K. Ito, H. Aoki, S. Uji, and T. Terashima: Phys. Rev. Lett. **98** (2007) 197001.
 - 26) R. S. Keizer, S. T. B. Goennenwein, T. M. Klapwijk, G. Miao, G. Xiao, and A. Gupta: Nature (London) **439** (2006) 825.
 - 27) M. S. Anwar, F. Czeschka, M. Hesselberth, M. Porcu, and J. Aarts: Phys. Rev. B **82** (2010) 100501(R).
 - 28) J. W. A. Robinson, J. D. S. Witt, and M. G. Blamire: Science **329** (2010) 59.
 - 29) T. S. Khaire, M. A. Khasawneh, W. P. Pratt, and N. O. Birge: Phys. Rev. Lett. **104** (2010) 137002.
 - 30) A. G. Lebed: JETP Lett. **44** (1986) 114.
 - 31) I. J. Lee, M. J. Naughton, G. M. Danner, and P. M. Chaikin: Phys. Rev. Lett. **78** (1997) 3555.
 - 32) J. Shinagawa, Y. Kurosaki, F. Zhang, C. Parker, S. E. Brown, D. Jérôme, J. B. Christensen, and K. Bechgaard: Phys. Rev. Lett. **98** (2007) 147002.
 - 33) S. Yonezawa, S. Kusaba, Y. Maeno, P. Auban-Senzier, C. Pasquier, K. Bechgaard, and D. Jérôme: Phys. Rev. Lett. **100** (2008) 117002.
 - 34) S. Yonezawa, S. Kusaba, Y. Maeno, P. Auban-Senzier, C. Pasquier, and D. Jérôme: J. Phys. Soc. Jpn. **77** (2008) 054712.
 - 35) P. A. Frigeri, D. F. Agterberg, A. Koga, and M. Sgrist: Phys. Rev. Lett. **92** (2004) 097001.

- 36) S. Fujimoto: J. Phys. Soc. Jpn. **76** (2007) 051008.
- 37) E. Bauer, G. Hilscher, H. Michor, C. Paul, E. W. Scheidt, A. Gribov, Y. Seropegin, H. Noël, M. Sigrist, and P. Rogl: Phys. Rev. Lett. **92** (2004) 027003.
- 38) N. Kimura, K. Ito, K. Saitoh, Y. Umeda, H. Aoki, and T. Terashima: Phys. Rev. Lett. **95** (2005) 247004.
- 39) A. P. Mackenzie and Y. Maeno: Rev. Mod. Phys. **75** (2003) 657.
- 40) A. J. Leggett: *Quantum Liquids: Bose Condensation And Cooper Pairing in Condensed-matter Systems* (Oxford Graduate Texts, Oxford, 2006) Appendix 6A.
- 41) Y. Tanaka and A. A. Golubov: Phys. Rev. Lett. **98** (2007) 037003.
- 42) A. P. Mackenzie, R. K. W. Haselwimmer, A. W. Tyler, G. G. Lonzarich, Y. Mori, S. Nishizaki, and Y. Maeno: Phys. Rev. Lett. **80** (1998) 161.
- 43) Z. Q. Mao, Y. Mori, and Y. Maeno: Phys. Rev. B **60** (1999) 610.
- 44) K. Ishida, H. Murakawa, H. Mukuda, Y. Kitaoka, Z. Q. Mao, and Y. Maeno: J. Phys. Chem. Solids **69** (2008) 3108.
- 45) K. Deguchi, Z. Q. Mao, H. Yaguchi, and Y. Maeno: Phys. Rev. Lett. **92** (2004) 047002.
- 46) T. M. Rice and M. Sigrist: J. Phys.:Condens. Matter **7** (1995) L643.
- 47) K. Ishida, H. Mukuda, Y. Kitaoka, K. Asayama, Z. Q. Mao, Y. Mori, and Y. Maeno: Nature (London) **396** (1998) 658.
- 48) G. M. Luke, Y. Fudamoto, K. M. Kojima, M. I. Larkin, J. Merrin, B. Nachumi, Y. J. Uemura, Y. Maeno, Z. Q. Mao, Y. Mori, H. Nakamura, and M. Sigrist: Nature (London) **394** (1998) 558.
- 49) M. Rice: Nature (London) **396** (1998) 627.
- 50) M. Sigrist: Prog. Theor. Phys. Suppl. **160** (2005) 1.
- 51) C. Kallin and A. J. Berlinsky: J. Phys. Condens. Matter **21** (2009) 164210.
- 52) C. Bergemann, A. P. Mackenzie, S. R. Julian, D. Forsythe, and E. Ohmichi: Adv. Phys. **52** (2003) 639.
- 53) F. Lichtenberg: Prog. Solid St. Chem. **30** (2002) 103.
- 54) Y. Maeno: *100 Years of Superconductivity* (Chapman & Hall / CRC of the Taylor&Francis Group, London, 2011) Sects. 4-8.
- 55) R. Balian and N. R. Werthamer: Phys. Rev. **131** (1963) 1553.
- 56) D. Vollhardt and P. Wölfle: *The Superfluid Phases of Helium 3* (Taylor&Francis Ltd, London, 1990)
- 57) O. Chmaissem, J. D. Jorgensen, H. Shaked, S. Ikeda, and Y. Maeno: Phys. Rev. B **57** (1998) 5067.
- 58) H. Mukuda, K. Ishida, Y. Kitaoka, K. Asayama, Z. Q. Mao, Y. Mori, and Y. Maeno: J. Phys. Soc. Jpn. **67** (1998) 3945.
- 59) J. A. Duffy, S. M. Hayden, Y. Maeno, Z. Mao, J. Kulda, and G. J. McIntyre: Phys. Rev. Lett. **85** (2000) 5412.
- 60) H. Mukuda, K. Ishida, Y. Kitaoka, K. Asayama, R. Kanno, and M. Takano: Phys. Rev. B **60** (1999) 12279.
- 61) K. Ishida, Y. Kitaoka, K. Asayama, S. Ikeda, S. Nishizaki, Y. Maeno, K. Yoshida, and T. Fujita: Phys. Rev. B **56** (1997) R505.
- 62) K. Ishida, H. Mukuda, Y. Minami, Y. Kitaoka, Z. Q. Mao, H. Fukazawa, and Y. Maeno: Phys. Rev. B **64** (2001) 100501(R).
- 63) H. Murakawa, K. Ishida, K. Kitagawa, H. Ikeda, Z. Q. Mao, and Y. Maeno: J. Phys. Soc. Jpn. **76** (2007) 024716.
- 64) H. Murakawa, K. Ishida, K. Kitagawa, Z. Q. Mao, and Y. Maeno: Phys. Rev. Lett. **93** (2004) 167004.
- 65) K. D. Nelson, Z. Q. Mao, Y. Maeno, and Y. Liu: Science **306** (2004) 1151. See also its Supporting Online Material.
- 66) M. Rice: Science **306** (2004) 1142.
- 67) J. Xia, P. T. Beyersdorf, M. M. Fejer, and A. Kapitulnik: Appl. Phys. Lett. **89** (2006) 062508.
- 68) J. Xia, Y. Maeno, P. T. Beyersdorf, M. M. Fejer, and A. Kapitulnik: Phys. Rev. Lett. **97** (2006) 167002.
- 69) J. Xia, V. Shelukhin, M. Karpovski, A. Kapitulnik, and A. Palevski: Phys. Rev. Lett. **102** (2009) 087004.
- 70) V. M. Yakovenko: Phys. Rev. Lett. **98** (2007) 087003.
- 71) J. Goryo: Phys. Rev. B **78** (2008) 060501(R).
- 72) R. Roy and C. Kallin: Phys. Rev. B **77** (2008) 174513.
- 73) R. M. Lutchyn, P. Nagornykh, and V. M. Yakovenko: Phys. Rev. B **80** (2009) 104508.
- 74) F. Kidwingira, J. D. Strand, D. J. V. Harlingen, and Y. Maeno: Science **314** (2006) 1267.
- 75) J. R. Kirtley, C. Kallin, C. W. Hicks, E.-A. Kim, Y. Liu, K. A. Moler, Y. Maeno, and K. D. Nelson: Phys. Rev. B **76** (2007) 014526.
- 76) C. W. Hicks, J. R. Kirtley, T. M. Lippman, N. C. Koshnick, M. E. Huber, Y. Maeno, W. M. Yuhasz, M. B. Maple, and K. A. Moler: Phys. Rev. B **81** (2010) 214501.
- 77) J. Jang, D. G. Ferguson, V. Vakaryuk, R. Budakian, S. B. Chung, P. M. Goldbart, and Y. Maeno: Science **331** (2011) 186.
- 78) V. O. Dolocan, C. Veauvy, F. Servant, P. Lejay, K. Hasselbach, Y. Liu, and D. Mailly: Phys. Rev. B **95** (2005) 097004.
- 79) M. Ichioka, Y. Matsunaga, and K. Machida: Phys. Rev. B **71** (2005) 172510.
- 80) S. Raghu, A. Kapitulnik, and S. A. Kivelson: Phys. Rev. Lett. **105** (2010) 136401.
- 81) Y. Tada, N. Kawakami, and S. Fujimoto: New J. Phys. **11** (2009) 055070.
- 82) Y. Tanaka, T. Yokoyama, A. V. Balatsky, and N. Nagaosa: Phys. Rev. B **79** (2009) 060505(R).
- 83) M. Sato and S. Fujimoto: Phys. Rev. B **79** (2009) 094504.
- 84) A. Furusaki, M. Matsumoto, and M. Sigrist: Phys. Rev. B **64** (2001) 054514.
- 85) S. Nishizaki, Y. Maeno, and Z. Mao: J. Phys. Soc. Jpn. **69** (2000) 572.
- 86) K. Ishida, H. Mukuda, Y. Kitaoka, Z. Q. Mao, Y. Mori, and Y. Maeno: Phys. Rev. Lett. **84** (2000) 5387.
- 87) M. A. Tanatar, S. Nagai, Z. Q. Mao, Y. Maeno, and T. Ishiguro: Phys. Rev. B **63** (2001) 064505.
- 88) K. Izawa, H. Takahashi, H. Yamaguchi, Y. Matsuda, M. Suzuki, T. Sasaki, T. Fukase, Y. Yoshida, R. Settai, and Y. Onuki: Phys. Rev. Lett. **86** (2001) 2653.
- 89) I. Bonalde, B. D. Yanoff, M. B. Salamon, D. J. V. Harlingen, E. M. E. Chia, Z. Q. Mao, and Y. Maeno: Phys. Rev. Lett. **85** (2000) 4775.
- 90) C. Lupien, W. A. MacFarlane, C. Proust, L. Taillefer, Z. Q. Mao, and Y. Maeno: Phys. Rev. Lett. **86** (2001) 5986.
- 91) K. Deguchi, Z. Q. Mao, and Y. Maeno: J. Phys. Soc. Jpn. **73** (2004) 1313.
- 92) T. Nomura and K. Yamada: J. Phys. Soc. Jpn. **71** (2002) 404.
- 93) D. F. Agterberg, T. M. Rice, and M. Sigrist: Phys. Rev. Lett. **78** (1997) 3374.
- 94) S. Souma, Y. Machida, T. Sato, T. Takahashi, H. Matsui, S.-C. Wang, H. Ding, A. Kaminski, J. C. Campuzano, S. Sasaki, and K. Kadowaki: Nature (London) **423** (2003) 65.
- 95) K. Kuroki, S. Onari, R. Arita, H. Usui, Y. Tanaka, H. Kontani, and H. Aoki: Phys. Rev. Lett. **101** (2008) 087004.
- 96) G. E. Volovik: JETP Lett. **58** (1993) 469.
- 97) I. Vekhter, P. J. Hirschfeld, J. P. Carbotte, and E. J. Nicol: Phys. Rev. B **59** (1999) 9023(R).
- 98) K. Deguchi, T. Ishiguro, and Y. Maeno: Rev. Sci. Instrum. **75** (2004) 1188.
- 99) H. Kusunose: J. Phys. Soc. Jpn. **73** (2004) 2512.
- 100) M. Udagawa, Y. Yanase, and M. Ogata: Phys. Rev. B **70** (2004) 184515.
- 101) A. Vorontsov and I. Vekhter: Phys. Rev. Lett. **96** (2006) 237001.
- 102) K. An, T. Sakakibara, R. Settai, Y. Onuki, M. Hiragi, M. Ichioka, and K. Machida: Phys. Rev. Lett. **104** (2010) 037002.
- 103) Y. Yanase and M. Ogata: J. Phys. Soc. Jpn. **72** (2003) 673.
- 104) M. W. Haverkort, I. S. Elfimov, L. H. Tjeng, G. A. Sawatzky, and A. Damascelli: Phys. Rev. Lett. **101** (2008) 026406.
- 105) E. J. Rozbicki, J. F. Annett, J.-R. Souquet, and A. P. Mackenzie: J. Phys.: Condens. Matter **23** (2011) 094201.
- 106) A. I. Ahonen, M. Krusius, and M. A. Paalanen: J. Low Temp. Phys. **25** (1976) 421.
- 107) K. Miyake: J. Phys. Soc. Jpn. **79** (2010) 024714.
- 108) Y. Hasegawa: J. Phys. Soc. Jpn. **72** (2003) 2456.
- 109) H. Mukuda, K. Ishida, Y. Kitaoka, K. Miyake, Z. Q. Mao, Y. Mori, and Y. Maeno: Phys. Rev. B **65** (2002) 132507.
- 110) L. Tewordt: Phys. Rev. Lett. **83** (1999) 1007.
- 111) L. Tewordt: J. Low Temp. Phys. **117** (1999) 1.

- 112) H. Y. Kee, Y. B. Kim, and K. Maki: Phys. Rev. B **61** (2000) 3584.
 113) H. Y. Kee, Y. B. Kim, and K. Maki: Phys. Rev. B **62** (2000) 5877.
 114) D. Fay and L. Tewordt: Phys. Rev. B **62** (2000) 4036.
 115) D. S. Hirashima: J. Phys. Soc. Jpn. **76** (2007) 034701.
 116) T. Nomura, D. S. Hirashima, and K. Yamada: J. Phys. Soc. Jpn. **77** (2008) 024701.
 117) I. I. Mazin and D. J. Singh: Phys. Rev. Lett. **79** (1997) 733.
 118) I. I. Mazin and D. J. Singh: Phys. Rev. Lett. **82** (1999) 4324.
 119) P. Monthoux and G. G. Lonzarich: Phys. Rev. B **59** (1999) 14598.
 120) P. Monthoux and G. G. Lonzarich: Phys. Rev. B **71** (2005) 054504.
 121) E. V. Kuz'min, S. G. Ovchinnikov, and I. O. Baklanov: Phys. Rev. B **61** (2000) 15392.
 122) T. Kuwabara and M. Ogata: Phys. Rev. Lett. **85** (2000) 4586.
 123) M. Sato and M. Kohmoto: J. Phys. Soc. Jpn. **69** (2000) 3505.
 124) K. Kuroki, M. Ogata, R. Arita, and H. Aoki: Phys. Rev. B **63** (2001) 060506(R).
 125) M. Ogata: J. Phys. Chem. Solids **63** (2002) 1329.
 126) T. Takimoto: Phys. Rev. B **62** (2000) R14641.
 127) G. Baskaran: Physica B **223-224** (1996) 490.
 128) J. Spałek: Phys. Rev. B **63** (2001) 104513.
 129) K. I. Wysokiński, G. Litak, J. F. Annett, and B. L. Görfrey: Phys. Stat. Sol. (b) **236** (2003) 325.
 130) S. Koikegami, Y. Yoshida, and T. Yanagisawa: Phys. Rev. B **67** (2003) 134517.
 131) T. Nomura and K. Yamada: J. Phys. Soc. Jpn. **69** (2000) 3678.
 132) T. Nomura and K. Yamada: J. Phys. Soc. Jpn. **71** (2002) 1993.
 133) T. Nomura and K. Yamada: J. Phys. Chem. Solids **63** (2002) 1337.
 134) C. Honerkamp and T. M. Rice: Physica C **388-389** (2003) 11.
 135) R. Werner: Phys. Rev. B **67** (2003) 014505.
 136) R. Arita, S. Onari, K. Kuroki, and H. Aoki: Phys. Rev. Lett. **92** (2004) 247006.
 137) K. Hoshihara and K. Miyake: J. Phys. Soc. Jpn. **74** (2005) 2679.
 138) T. Oguchi: Phys. Rev. B **51** (1995) 1385.
 139) D. J. Singh: Phys. Rev. B **52** (1995) 1358.
 140) A. P. Mackenzie, S. R. Julian, A. J. Diver, G. J. McMullan, M. P. Ray, G. G. Lonzarich, Y. Maeno, S. Nishizaki, and T. Fujita: Phys. Rev. Lett. **76** (1996) 3786.
 141) S. Nakatsuji, S.-I. Ikeda, and Y. Maeno: J. Phys. Soc. Jpn. **66** (1997) 1868.
 142) S. Nakatsuji and Y. Maeno: Phys. Rev. Lett. **84** (2000) 2666.
 143) Y. Sidis, M. Braden, P. Bourges, B. Hennion, S. NishiZaki, Y. Maeno, and Y. Mori: Phys. Rev. Lett. **83** (1999) 3320.
 144) T. Nomura and K. Yamada: J. Phys. Soc. Jpn. **69** (2000) 1856.
 145) I. Eremin, D. Manske, and K. H. Bennemann: Phys. Rev. B **65** (2002) 220502(R).
 146) Y. Hasegawa, K. Machida, and M. Ozaki: J. Phys. Soc. Jpn. **69** (2000) 336.
 147) M. E. Zhitomirsky and T. M. Rice: Phys. Rev. Lett. **87** (2001) 057001.
 148) T. Moriya: *Spin Fluctuations in Itinerant Electron Magnetism* (Springer Verlag, Berlin, 1985)
 149) N. E. Bickers, D. J. Scalapino, and S. R. White: Phys. Rev. Lett. **62** (1989) 961.
 150) D. J. Scalapino, E. Loh, and J. E. Hirsch: Phys. Rev. B **34** (1986) 8190.
 151) A. V. Chubukov: Phys. Rev. B **48** (1993) 1097.
 152) J. Feldman, H. Knörrer, R. Sinclair, and E. Trubowitz: Helv. Phys. Acta **70** (1997) 154.
 153) Y. Yanase, T. Jujo, T. Nomura, H. Ikeda, T. Hotta, and K. Yamada: Phys. Reports **387** (2003) 1.
 154) C. Honerkamp and M. Salmhofer: Phys. Rev. Lett. **87** (2001) 187004.
 155) T. Nomura: J. Phys. Soc. Jpn. **74** (2005) 1818.
 156) K. Miyake and O. Narikiyo: Phys. Rev. Lett. **83** (1999) 1423.
 157) T. Nomura, H. Ikeda, and D. S. Hirashima: J. Phys. Chem. Solids **69** (2008) 3352.
 158) K. K. Ng and M. Sgrist: Europhys. Lett. **49** (2000) 473.
 159) J. F. Annett, G. Litak, B. L. Györfy, and K. I. Wysokiński: Phys. Rev. B **73** (2006) 134501.
 160) Y. Yoshioka and K. Miyake: J. Phys. Soc. Jpn. **78** (2009) 074701.
 161) H. Iwasawa, Y. Yoshida, I. Hase, S. Koikegami, H. Hayashi, J. Jiang, K. Shimada, H. Namatame, M. Taniguchi, and Y. Aiura: Phys. Rev. Lett. **105** (2010) 226406.
 162) E. Helfand and N. R. Werthamer: Phys. Rev. **147** (1966) 288.
 163) N. R. Werthamer, E. Helfand, and P. C. Hohenberg: Phys. Rev. **147** (1966) 295.
 164) K. Maki, G. F. Wang, and H. Won: J. Supercond. **12** (1999) 551.
 165) A. G. Lebed and N. Hayashi: Physica C **341-348** (2000) 1677.
 166) S. Kittaka, T. Nakamura, Y. Aono, S. Yonezawa, K. Ishida, and Y. Maeno: J. Phys.: Conf. Ser. **150** (2009) 052112.
 167) K. Machida and M. Ichioka: Phys. Rev. B **77** (2008) 184515.
 168) C.-H. Choi: J. Korean Phys. Soc. **56** (2010) 933.
 169) R. Joynt and L. Taillefer: Rev. Mod. Phys. **74** (2002) 235.
 170) K. Machida and T. Ohmi: J. Phys. Soc. Jpn. **67** (1998) 1122.
 171) K. Deguchi, M. A. Tanatar, Z. Q. Mao, T. Ishiguro, and Y. Maeno: J. Phys. Soc. Jpn. **71** (2002) 2839.
 172) N. H. van Dijk, A. de Visser, J. J. M. Franse, and L. Taillefer: J. Low Temp. Phys. **93** (1993) 101.
 173) S. Kittaka, T. Nakamura, Y. Aono, S. Yonezawa, K. Ishida, and Y. Maeno: Phys. Rev. B **80** (2009) 174514.
 174) H. Yaguchi, T. Akima, Z. Mao, Y. Maeno, and T. Ishiguro: Phys. Rev. B **66** (2002) 214514.
 175) K. Tenya, S. Yasuda, M. Yokoyama, H. Amitsuka, K. Deguchi, and Y. Maeno: J. Phys. Soc. Jpn. **75** (2006) 023702.
 176) Z. Q. Mao, Y. Maeno, S. NishiZaki, T. Akima, and T. Ishiguro: Phys. Rev. Lett. **84** (2000) 991.
 177) R. P. Kaur, D. F. Agterberg, and H. Kusunose: Phys. Rev. B **72** (2005) 144528.
 178) V. P. Mineev: Phys. Rev. B **77** (2008) 064519.
 179) M. Udagawa, Y. Yanase, and M. Ogata: J. Phys. Soc. Jpn. **74** (2005) 2905.
 180) Y. Maeno, T. Ando, Y. Mori, E. Ohmichi, S. Ikeda, S. NishiZaki, and S. Nakatsuji: Phys. Rev. Lett. **81** (1998) 3765.
 181) Z. Q. Mao, Y. Maeno, and H. Fukazawa: Mat. Res. Bull. **35** (2000) 1813.
 182) Y. A. Ying, Y. Xin, B. W. Clouser, E. Hao, N. E. Staley, R. J. Myers, L. F. Allard, D. Fobes, T. Liu, Z. Q. Mao, and Y. Liu: Phys. Rev. Lett. **103** (2009) 247004.
 183) H. Yaguchi, M. Wada, T. Akima, Y. Maeno, and T. Ishiguro: Phys. Rev. B **67** (2003) 214519.
 184) Z. Q. Mao, K. D. Nelson, R. Jin, Y. Liu, and Y. Maeno: Phys. Rev. Lett. **87** (2001) 037003.
 185) M. Kawamura, H. Yaguchi, N. Kikugawa, Y. Maeno, and H. Takayanagi: J. Phys. Soc. Jpn. **74** (2005) 531.
 186) H. Yaguchi, K. Takizawa, M. Kawamura, N. Kikugawa, Y. Maeno, T. Meno, T. Akazaki, K. Semba, and H. Takayanagi: J. Phys. Soc. Jpn. **75** (2006) 125001.
 187) T. Ando, T. Akima, Y. Mori, and Y. Maeno: J. Phys. Soc. Jpn. **68** (1999) 1651.
 188) J. Hooper, Z. Q. Mao, K. D. Nelson, Y. Liu, M. Wada, and Y. Maeno: Phys. Rev. B **70** (2004) 014510.
 189) S. Kittaka, T. Nakamura, H. Yaguchi, S. Yonezawa, and Y. Maeno: J. Phys. Soc. Jpn. **78** (2009) 064703.
 190) M. Wada, H. Yaguchi, M. Yoshioka, and Y. Maeno: J. Phys. Chem. Solids **63** (2002) 1013.
 191) M. Sgrist and H. Monien: J. Phys. Soc. Jpn. **70** (2001) 2409.
 192) M. Matsumoto, C. Belardinelli, and M. Sgrist: J. Phys. Soc. Jpn. **72** (2003) 1623.
 193) H. Kaneyasu and M. Sgrist: J. Phys. Soc. Jpn. **79** (2010) 053706.
 194) H. Kaneyasu, N. Hayashi, B. Gut, K. Makoshi, and M. Sgrist: J. Phys. Soc. Jpn. **79** (2010) 104705.
 195) S. Kittaka, H. Taniguchi, S. Yonezawa, H. Yaguchi, and Y. Maeno: Phys. Rev. B **81** (2010) 180510(R).
 196) H. Yaguchi, S. Kittaka, and Y. Maeno: J. Phys.: Conf. Ser. **150** (2009) 052285.
 197) S. Kittaka, H. Yaguchi, and Y. Maeno: J. Phys. Soc. Jpn. **78** (2009) 103705.

- 198) N. Shirakawa, K. Murata, S. Nishizaki, Y. Maeno, and T. Fujita: Phys. Rev. B **56** (1997) 7890.
- 199) D. Forsythe, S. R. Julian, C. Bergemann, E. Pugh, M. J. Steiner, P. L. Alireza, G. J. McMullan, F. Nakamura, R. K. W. Haselwimmer, I. R. Walker, S. S. Saxena, G. G. Lonzarich, A. P. Mackenzie, Z. Q. Mao, and Y. Maeno: Phys. Rev. Lett. **89** (2002) 166402.
- 200) H. Yaguchi, S. Kawada, H. Watanabe and S. Suzuki: J. Phys. Soc. Jpn. **79** (2010) 125004.
- 201) R. Fittipaldi, A. Vecchione, S. Fusanobori, K. Takizawa, H. Yaguchi, J. Hooper, R. S. Perry, and Y. Maeno: J. Cryst. Growth **282** (2005) 152.
- 202) R. Ciancio, H. Pettersson, J. Börjesson, S. Lopatin, R. Fittipaldi, A. Vecchione, S. Kittaka, Y. Maeno, S. Pace, and E. Olsson: App. Phys. Lett. **95** (2009) 142507.
- 203) R. Ciancio, J. Börjesson, H. Pettersson, R. Fittipaldi, D. Zola, A. Vecchione, M. Polichetti, S. Kittaka, Y. Maeno, S. Pace, and E. Olsson: Phys. Rev. B **80** (2009) 054110.
- 204) S. Kittaka, S. Fusanobori, S. Yonezawa, H. Yaguchi, Y. Maeno, R. Fittipaldi, and A. Vecchione: Phys. Rev. B **77** (2008) 214511.
- 205) S. Kittaka, S. Yonezawa, H. Yaguchi, Y. Maeno, R. Fittipaldi, A. Vecchione, J.-F. Mercure, A. Gibbs, R. S. Perry, and A. P. Mackenzie: J. Phys.: Conf. Ser. **150** (2009) 052113.
- 206) R. Fittipaldi, A. Vecchione, R. Ciancio, S. Pace, M. Cuoco, D. Stornaiuolo, D. Born, F. Tafuri, E. Olsson, S. Kittaka, H. Yaguchi, and Y. Maeno: Europhys. Lett. **83** (2008) 27007.
- 207) J. Hooper, M. Zhou, Z. Q. Mao, Y. Liu, R. Perry, and Y. Maeno: Phys. Rev. B **73** (2006) 132510.
- 208) S.-I. Ikeda, N. Shirakawa, T. Yanagisawa, Y. Yoshida, S. Koikegami, S. Koike, M. Kosaka, and Y. Uwatoko: J. Phys. Soc. Jpn. **73** (2004) 1322.
- 209) H. Yaguchi, R. S. Perry, and Y. Maeno: AIP Conf. Proc. **850** (2006) 1203.
- 210) S. Kittaka, H. Yaguchi, and Y. Maeno: Physica C **470** (2010) S728.
- 211) Y. Yanase: J. Phys. Soc. Jpn. **79** (2010) 084701.
- 212) A. P. Schnyder, S. Ryu, A. Furusaki, and A. W. W. Ludwig: Phys. Rev. B **78** (2008) 195125.
- 213) Y. Tanaka, M. Sato, and N. Nagaosa: arXiv:1105.4700.
- 214) S. Kashiwaya, H. Kashiwaya, H. Kambara, T. Furuta, H. Yaguchi, Y. Tanaka, and Y. Maeno: Phys. Rev. Lett. **107** (2011) 077003.
- 215) Y. S. Hor, A. J. Williams, J. G. Checkelsky, P. Roushan, J. Seo, Q. Xu, H. W. Zandbergen, A. Yazdani, N. P. Ong, and R. J. Cava: Phys. Rev. Lett. **104** (2010) 057001.
- 216) M. Kriener, K. Segawa, Z. Ren, S. Sasaki, and Y. Ando: Phys. Rev. Lett. **106** (2011) 127004.
- 217) S. Sasaki, M. Kriener, K. Segawa, K. Yada, Y. Tanaka, M. Sato, and Y. Ando: Phys. Rev. Lett. **107** (2011) 217001.
- 218) Y. Tanaka and S. Kashiwaya: Phys. Rev. Lett. **74** (1995) 3451.
- 219) Y. Tanaka and S. Kashiwaya: Phys. Rev. B **70** (2004) 012507.
- 220) Y. Asano, Y. Tanaka, A. A. Golubov, and S. Kashiwaya: Phys. Rev. Lett. **99** (2007) 067005.
- 221) Y. Tanaka, A. A. Golubov, S. Kashiwaya, and M. Ueda: Phys. Rev. Lett. **99** (2007) 037005.
- 222) H. Kambara, S. Kashiwaya, H. Yaguchi, Y. Asano, Y. Tanaka, and Y. Maeno: Phys. Rev. Lett. **101** (2008) 267003.
- 223) H. Kambara, T. Matsumoto, H. Kashiwaya, S. Kashiwaya, H. Yaguchi, Y. Asano, Y. Tanaka, and Y. Maeno: J. Phys. Soc. Jpn. **79** (2010) 074708.
- 224) S. Kashiwaya, H. Kambara, H. Kashiwaya, T. Furuta, H. Yaguchi, Y. Asano, Y. Tanaka, and Y. Maeno: Physica C **470** (2010) S736.
- 225) T. Nakamura, R. Nakagawa, T. Yamagishi, T. Terashima, S. Yonezawa, M. Sigrist, and Y. Maeno: Phys. Rev. B **84** (2011) 060512(R).
- 226) R. Jin, Y. Zadorozhny, Y. Liu, D. G. Schlom, Y. Mori, and Y. Maeno: Phys. Rev. B **59** (1999) 4433.
- 227) G. E. Volovik and V. P. Mineev: JETP Lett. **24** (1976) 561.
- 228) M. C. Cross and W. F. Brinkman: J. Low Temp. Phys. **27** (1977) 683.
- 229) M. Yamashita, K. Izumina, A. Matsubara, Y. Sasaki, O. Ishikawa, T. Takagi, M. Kubota, and T. Mizusaki: Phys. Rev. Lett. **101** (2008) 025302.
- 230) S. B. Chung, H. Bluhm, and E.-A. Kim: Phys. Rev. Lett. **99** (2007) 197002.
- 231) V. Vakaryuk and A. J. Leggett: Phys. Rev. Lett. **103** (2009) 057003.
- 232) M. Sigrist and K. Ueda: Rev. Mod. Phys. **63** (1991) 239.
- 233) V. P. Mineev and K. V. Samokhin: *Introduction to Unconventional Superconductivity* (Gordon and Breach Science Publishers, New York, 1999)
- 234) I. I. Mazin, D. J. Singh, M. D. Johannes, and M. H. Du: Phys. Rev. Lett. **101** (2008) 057003.